THE FLORIDA STATE UNIVERSITY

COLLEGE OF ARTS AND SCIENCES

VERIFICATION OF A NUMERICAL OCEAN MODEL OF THE ARABIAN SEA

by

RAY C. SIMMONS

A Thesis submitted to the
Department of Oceanography
in partial fulfillment of the
requirments for the degree of
Master of Science

Approved:

James J. O'Brien
Professor Directing Thesis

George Weatherly

William M. Sanders

Chairman, Department of Oceanography

Chairman, Department of Oceanography

Fall Semester, 1987

ABSTRACT

A case study evaluating the predictive capability of an upper layer circulation model of the northwest Indian Ocean is presented. The model is a nonlinear, reduced gravity model incorporating realistic boundary geometry and is forced by actual wind observations. Model results for the fall of 1985 are compared to, and evaluated against, U.S. Navy bathythermograph and NOAA satellite data collected during August - November 1985. An assessment of the model's ability to predict correctly the circulation structure is made. Wind observations were converted to wind stress for model forcing by a procedure developed by Legler and Navon (1987). The model is only moderately successful in reproducing the structure of the large, rather homogeneous pool of water located off the Arabian Peninsula in September. However, the model behaves remarkably well in the dynamically active region around Socotra. Major fronts and eddies frequently observed in the region during the transition period between the southwest and the northeast monsoon appear in the 1985 model results and compare well, both temporally and spacially, with the observational data. Thus, given accurate wind information, the model appears highly effective in dynamically active regions, and demonstrates potential as a useful prognostic tool for evaluation of the Arabian Sea when real time winds become available.

the Arabian Sea when real time winds become available.

ACKNOWLEDGEMENTS

Modern ocean modelling has evolved to the point where a consolidated effort on the part of many is necessary to achieve success. As such, I wish to express my gratitude to the many individuals who participated and assisted me with this project.

Support was provided by the Office of Naval Research, the Secretary of the Navy Research Chair in Oceanography and the Institute of Naval Oceanography. Supplemental support was provided by the NASA Oceanic Processes Branch as part of the NASA Traineeship Grant. TOGA wind data were provided by NOAA.

Thanks to Mr. B. J. Cagle of the ONR Western Regional Office, who provided the motivation for this work and arranged for the Navy BT data, Mr. R. Whritner of the Scripps Satellite Oceanography Facility, who provided the satellite SST imagery, and Dr. I. M. Navon, who was instrumental in the development of the objective analysis used on the wind data.

Personal thanks to Dr. M. E. Luther, whose guidance and assistance were essential to my success, and to Drs. G. Weatherly and W. Landing for their efforts as members of my thesis committee. Special thanks also to Mr. J. Merritt for his expert programming assistance, the members of the Mesoscale Air-Sea Interaction Group for their helpful comments, and especially Mrs. Rita Kuyper for her masterful performance during the tedious typing phase of the project.

Finally, I wish to express my deepest appreciation to Dr. J. J. O'Brien who has been much more than a major professor. His encouragement and dedicated support have prepared me well as I begin my Naval oceanography career. I am most fortunate for having had this opportunity to study under him, and thank Dr. W. S. Wilson of NASA for having suggested and made this possible.

TABLE OF CONTENTS

LIST OF FIGURES

by the darker shading, is observed in the upper center of the image, south of and offshore of the Arabian Peninsula between

blocked by the intensified North Socotra Cyclonic Eddy. The waves build east of Socotra (thickening of the ULT) and by the beginning

south immediately off the coast, with a thinner layer extending offshore to about 62°E..... 37

measured east from 51°E. The North Socotra Warm Eddy at about 220km, and Socotra Eddy at about 680km, are distinctly separated

Fig. 19. The southwest quadrant of the NOAA-8 AVHRR image of 30

appearing at about 380km. The BT data clearly shows a 50 - 60km region of upwelling immediately off the coast of Oman, which is

Fig. 25. The 18°C isotherm depth (meters) for 1 - 10 October 1985. Contours are generated from the BT data (solid contours) when sufficient readings are available, and are estimated (dashed contours) where BT data are deficient. Numerous dynamic features can be observed surrounding Socotra Island. The great whirl is seen penetrating from the south, while indications of the Socotra Eddy are observed by a deepening of the isotherm east of Socotra. The strong North Socotra Cyclonic Eddy is observed to the northeast of Socotra, with a relatively cool tongue extending to the south immediately east of the island, and separating the great whirl and Socotra Eddies. Weak deepening of the thermocline (warming) is observed to the north and west of Socotra, while intense fronts are observed off the coast of Somalia, northeast of Socotra, and between the Socotra Eddy and the intense North Socotra Cyclonic Eddy..... 51

Fig. 26. Model response for 6 October 1985. The three major anticyclonic eddies - the great whirl, North Socotra Warm Eddy and Socotra Eddy - as well as the North Socotra Cyclonic Eddy are all well established around Socotra Island. A thin layer (cool) tongue extends south of the North Socotra Cyclonic Eddy east of Socotra, separating the three anticyclonic eddies from each other. Strong extends south of the North Socotra Cyclonic Eddy east of Socotra, separating the three anticyclonic eddies from each other. Strong

(cool) tongue extending south from it along the eastern shore of Socotra. The Socotra Eddy has drifted westward and begun to

Fig. 31. Profiles of the BT 18°C isotherm for 20 - 30 October 1985 (dashed line) and model ULT for 26 October 1985 (solid line), along

boundaries separating these major features at 200km, 400km, and 700km respectively..... 61

INTRODUCTION

Forced by the semiannually reversing northeast and southwest monsoonal winds, circulation patterns of the northwest Indian Ocean, the Arabian Sea, have intrigued oceanographers for many years. Of particular interest is the Somali Current, unique to the region, with its reversing flow and dynamically active circulation structure, characterized by a very complex system of eddies and fronts.

During the northern winter, the northeast monsoon drives northeasterly winds and a corresponding southward boundary current along the Somali coast. As winter transitions into spring, the northeast monsoon relaxes and the coastal current reverses along Kenya and southern Somalia. By mid-April, the Southern Hemisphere trade winds extend well to the northwest and a northward surface current flows to the equator, where it turns offshore and recirculates to the south forming a southern gyre. By May the winds reverse all along the Somali coast and form a jet-like structure (Findlater, 1971), analogous to an oceanic western boundary current, which is confined in the west by the highlands of Kenya and Ethiopia and remains over land at very low latitudes. In June, the core of this atmospheric jet crosses the coast at about 8°N and becomes very strong. A second gyre forms between 4°N and 10°N to which Findlay, in 1866, attached the name "great whirl." This two gyre system intensifies throughout June forms between 4°N and 10°N to which Findlay, in 1866, attached the name "great whirl." This two gyre system intensifies throughout June and is well established by mid to late July, when the winds again

begin to weaken and the two gyres coalesce and begin a slow migration to the north. Numerous modelling efforts, in conjunction with extensive observations (Swallow & Fieux (1982); Schott (1983); Swallow, et al. (1983); Knox & Anderson (1985)), have shown this dynamic structure along the African coast to be relatively consistant year-to-year during the southwest monsoon.

In October, the winds begin to reverse, indicating the onset of the northeast monsoon, and the southward Somali current again develops. Prior to a complete wind shift however, a complicated dynamic circulation structure develops around Socotra Island and along the Arabian Peninsula. To date, little attention has been focused on this fall circulation structure, however Cagle and Whritner (1981) used satellite infrared imagery to observe and describe a number of the complicated dynamic features of the region. They concluded from their study that the various eddies and wedges found in the northern Arabian Sea during the breakdown of the southwest monsoon are a response to wind forcing and topographic features associated with the coastal geometry. The study presented here investigates these fall dynamic features, with particular emphasis centered on the northwest Arabian Sea, north of Socotra, during September - November 1985.

Cox (1970) was the first to attempt a large-scale numerical model of the Indian Ocean, using an early version of the Bryan-Cox or GFDL model. The model, driven by idealizations of observed wind stress and temperature-salinity data, and integrated over two centuries.
model. The model, driven by idealizations of observed wind stress and temperature-salinity data, and integrated over two centuries,

reproduced the reversal of the Somali Current and most of the other large-scale circulation features of the region, but limited resolution prohibited simulation of many small-scale features. This was an important result however, as it was inferred from this investigation that the rapid spin-up of the Somali Current at the beginning of the southwest monsoon was due to local winds, as compared to Lighthill's (1969) result which hypothesized that the Somali Current is remotely forced by westward propogating equatorial Rossby waves generated by winds within the Indian Ocean interior. Anderson and Rowlands (1976) investigated this problem and were able to show analytically, that local forcing is important initially, but that remote forcing effects become important over time. Cox (1976) was able to confirm this with his model, but also showed that friction and nonlinear effects modify their result, and that nonlinear horizontal shearing instabilities are able to produce eddies similar to those observed in the Somali Current system.

The northward migration of the great whirl was investigated by Hurlburt and Thompson (1976) using a two-layer numerical model in which they showed that nonlinear eddies, formed at the equator by an impulsively applied wind stress, could indeed move northward along the coast as a result of advective effects. Cox (1979) extended this investigation by incorporating effects of boundary orientation on the northward advection of the eddies and determined that migration is dependent upon boundary slope, and is arrested for slopes of greater northward advection of the eddies and determined that migration is dependent upon boundary slope, and is arrested for slopes of greater

than 45°. The net result of these studies was Cox's (1981) conclusion that eddy movement is dependent upon advection of vorticity, vortex stretching, the beta effect and the wind stress curl.

Further numerical studies have been conducted by Anderson and Moore (1979), who took the Somali current to be a free inertial cross-equatorial jet, remotely forced by the Southern Hemisphere trade winds, and found reasonable separation latitudes for the southern gyre of the Somali Current. Lin and Hurlburt (1981) used a reduced gravity model with an impulsively applied wind, parallel to the coast and constant alongshore, to reproduce two equatorial eddies that subsequently migrated northward. Anderson (1981), again with a reduced gravity model, showed that the southern-most gyre could be generated by the northwest penetration of the Southern Hemisphere trade winds at the onset of the southwest monsoon, while the northern gyre results from the departure from the Somali Coast around 9°N of Findlater's low level wind jet. Observations, described in Schott and Quadfasel (1982), further indicate that the local curl of the wind stress in the development of the low-level jet also plays a significant role in formation of the great whirl.

The above described large-scale features are repeatable phenomena in many numerical studies. Numerous small-scale features - eddies, wedges and fronts - are less repeatable in models and appear to be highly dependent upon the structure of the wind forcing. A number of observations have described these features along the African to be highly dependent upon the structure of the wind forcing. A number of observations have described these features along the African

coast during the southwest monsoon (Bruce (1973, 1979, 1983); Brown, Bruce and Evans (1980)). Far less attention has been devoted to the eddies and fronts found around and to the north of Socotra as the northeast Somali Current breaks down and transitions into the southwest Somali Current during the northern fall.

Luther and O'Brien (1985) developed the real-geometry model used in this study and forced it with climatological winds to reproduce most of the observed features of the Somali Current system. The presence of a large, time-varying region of wind stress curl within, and just offshore of, the boundary region, as well as the inclusion of the entire seasonal cycle, was found to be critical for the accurate simulation of observed circulation patterns. Further study using the same model driven by the monthly mean winds from the First GARP Global Experiment and monthly mean climatological winds, again reproduced the observed features of the region, and an assessment of the effects of various forcing mechanisms-spacial and temporal inhomogeneity of the winds, negative vorticity input by the wind stress curl, and differential Ekman pumping-on the generation and decay of the two-gyre system were reported by Luther, O'Brien and Meng (1985).

In the present study, actual observed winds for the period 1954 through 1985 are used to force the model and generate the resultant dynamic response. Features present north of and around Socotra during the decay of the northeast Somali Current are then analyzed and compared to actual observations made during this dynamically active the decay of the northeast Somali Current are then analyzed and compared to actual observations made during this dynamically active

period, September - November 1985, for which U.S. Navy expendable bathythermograph (XBT) and NOAA Advanced Very High Resolution Radiometer (AVHRR) satellite images were collected and analyzed for the region.

In the next section, the model is briefly described, followed by a description of the available wind and oceanographic data, and finally an evaluation and assessment of the model's ability to effectively predict Arabian Sea dynamics, given reasonably accurate actual winds, is made based on the available XBT and satellite data.

THE MODEL

The nonlinear reduced gravity transport equations are used to model the upper ocean response to an applied wind stress. To accomodate the latitudinal extent of the model, spherical coordinates are used, with ϕ (longitude) increasing eastward and θ (latitude) increasing northward. Eastward and northward upper layer transport components are defined by $U=uH$ and $V=vH$, respectively, where u,v are the depth-independent upper layer ϕ,θ velocity components, and H is the upper layer thickness. The equations are:

$$\frac{\partial U}{\partial t} + \frac{1}{a \cos\theta}\frac{\partial}{\partial \phi}\left(\frac{U^2}{H}\right) + \frac{1}{a}\frac{\partial}{\partial \theta}\left(\frac{UV}{H}\right) - (2\Omega \sin\theta)V =$$

$$= \frac{-g'}{2a \cos\theta}\frac{\partial H^2}{\partial \phi} + \frac{\tau^{(\phi)}}{\rho_1} + A\nabla^2 U \qquad (1a)$$

$$\frac{\partial V}{\partial t} + \frac{1}{a \cos\theta}\frac{\partial}{\partial \phi}\left(\frac{UV}{H}\right) + \frac{1}{a}\frac{\partial}{\partial \theta}\left(\frac{V^2}{H}\right) + (2\Omega \sin\theta)U =$$

$$= \frac{-g'}{2a}\frac{\partial H^2}{\partial \theta} + \frac{\tau^{(\theta)}}{\rho_1} + A\nabla^2 V \qquad (1b)$$

$$\frac{\partial H}{\partial t} + \frac{1}{a \cos\theta}\left[\frac{\partial U}{\partial \phi} + \frac{\partial}{\partial \theta}(V \cos\theta)\right] = 0 \qquad (1c)$$

where $g' = \dfrac{g(\rho_2-\rho_1)}{\rho_2}$ is the reduced gravitational acceleration, a is the Earth's radius, Ω is the Earth's rotation rate, A is a kinematic eddy viscosity, and wind stress, $\tau = \{\tau^{\phi},\tau^{\theta}\}$, is applied as a body

force over the upper layer (Charney, 1955). Using the transport form of the reduced gravity equations provides the advantage that the equation of continuity, (1c) is linear. Additionally, the discretization of the advective terms of (1a) and (1b) involves spacial averaging of the dependent variables, thus improving numerical stability of the solution.

Model geometry, shown in Fig. 1, simulates the geography of the Arabian Sea from 40°E to 73°E and from 10°S to 25°N. Boundary conditions along all solid boundaries are non-slip, where:

$$u = v = 0.$$

Open boundaries are located along the entire southern boundary and along the eastern boundary from 5°S to the equator. Boundary conditions here are a variation of the Sommerfeld radiation condition developed by Camerlango and O'Brien (1980). Solid boundaries are located along all remaining boundaries including the southeastern corner of the model, which simulates the Chagos Archipelago; the region from the equator to the Gulf of Khambat, which simulates the Laccadive and Maldive Islands; and the shallow bank regions around the Seychelles and Socotra Islands. Deep channels within island chains are ignored.

Equations (1a), (1b) and (1c) are solved numerically on a 135 x

Equations (1a), (1b) and (1c) are solved numerically on a 135 x

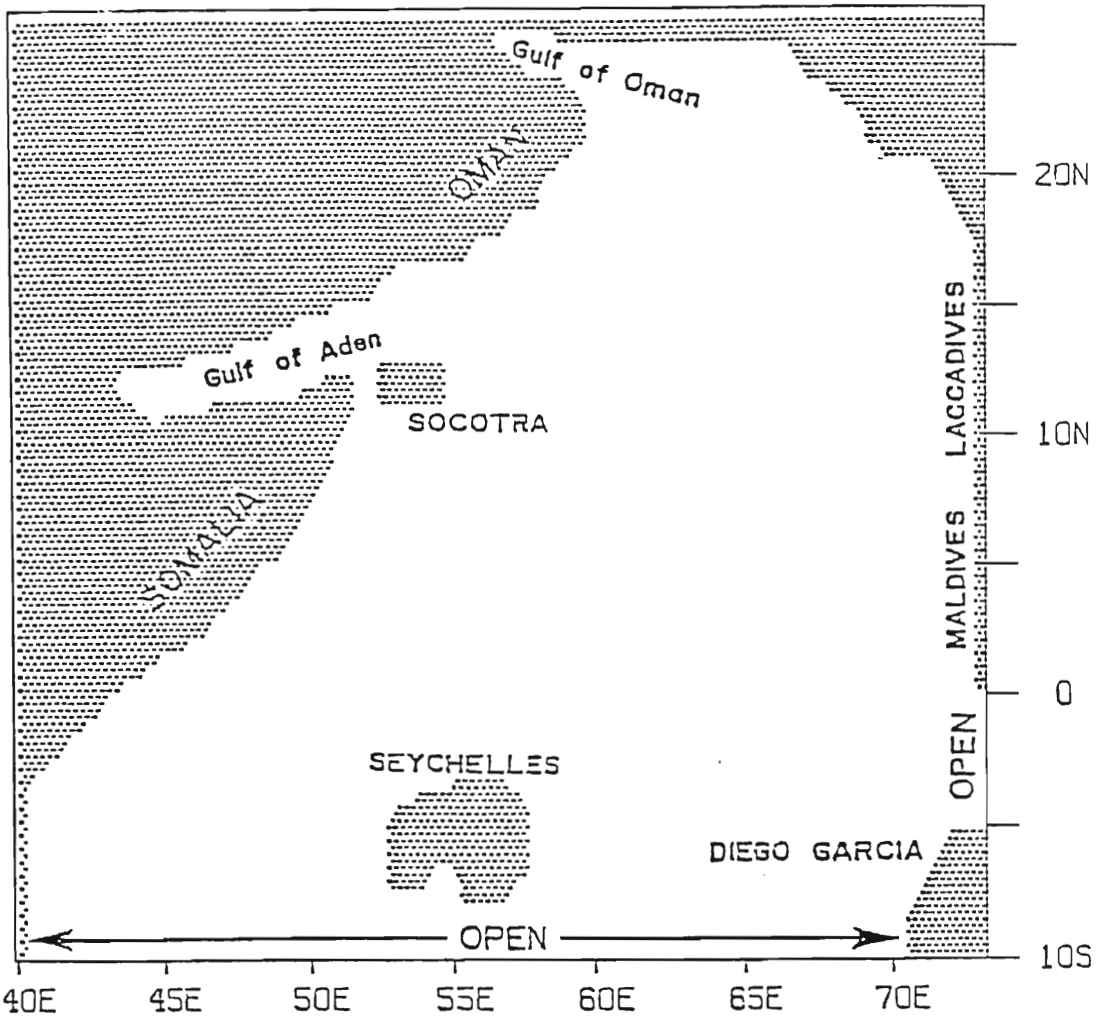

Fig. 1. Model geometry. Shaded regions indicate land boundaries. Significant geographic features surrounding the Arabian Sea, including major islands of Socotra, the Seychelles, Laccadives, Maldives, and Chagos Archipelgo, and associated shoal waters, are represented as solid land masses. The Straits of Hormuz and Bab-al-Mandab are assumed closed. while open boundaries exist along the southern
major islands of Socotra, the Seychelles, Laccadives, Maldives, and Chagos Archipelgo, and associated shoal waters, are represented as solid land masses. The Straits of Hormuz and Bab-al-Mandab are assumed closed, while open boundaries exist along the southern
boundary at 10°S and the eastern boundary from 5°S to the equator.

74 finite difference mesh which is staggered in space as shown in Fig. 2. Model resolution is 1/8° zonally ($\Delta\phi$) and 1/4° meridionally ($\Delta\theta$). The equations are integrated in time using a leapfrog finite difference scheme, with a forward time difference used every 99th time step to eliminate the computational mode. The model time step is 30 minutes. Advective terms are computed by first averaging adjacent U, V and H values in space to form the desired product at the appropriate mesh point, and then forming the standard, second-order accurate, centered finite difference approximation. Spacial averaging suppresses nonlinear growth of numerical noise within the model. In the linearized form of the reduced gravity equations, linear phase speed for the particular baroclinic mode to be modeled, $C = (g'H_o)^{1/2}$, must be prescribed. In the nonlinear form, there is no analogous phase speed parameter, only g'; however, in the numerical solution of equations (1a), (1b), and (1c), initial upper layer thickness, H_o, must be defined. This is analogous to prescribing an initial phase speed, although it does not remain constant, as variations of H are large with respect to H_o. Average upper layer thickness varies due to inflow/outflow through the open boundaries during the seasonal cycle. The other free parameter in the model is A, the kinematic eddy viscosity, which serves to damp out grid-scale noise in the model and prevents this noise from growing through nonlinear interactions.

For results presented here, H_o=200m, A=0.75 * 10^3 m^2s^{-1} and g'=0.03ms^{-2}. The model was integrated from rest, beginning at 0001Z

For results presented here, H_o=200m, A=0.75 * 10^3 m^2s^{-1} and g'=0.03ms^{-2}. The model was integrated from rest, beginning at 0001Z

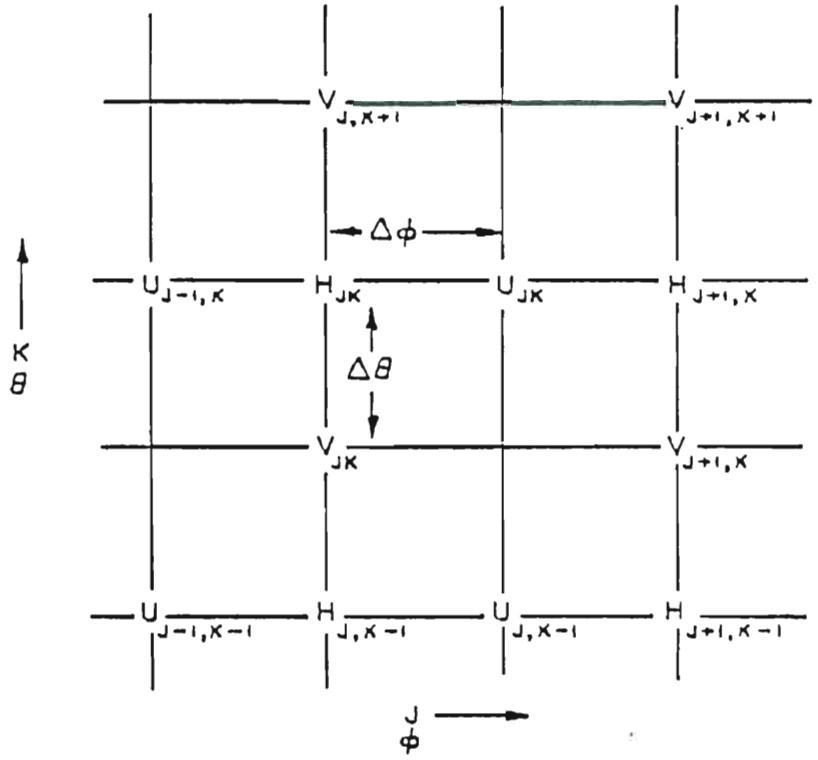

Fig. 2. Model grid. The model uses a staggered, Arakawa C-grid, upon which the model quantitites, U, V, and H, are defined. Resolution is 1/8° in the zonal direction ($\Delta\phi$) and 1/4° in the meridional direction ($\Delta\theta$).

on 16 December 1984, using an exponential taper with an e-folding time of 20 days to reduce the initial transients. The monthly mean winds for 1985 were applied repeatedly for 4 years until a steady seasonal cycle was obtained. The results presented here are from the fourth year of the simulation. For simplicity, the model year is 360 days, with each month containing 30 days.

THE DATA

a) Wind Forcing

The model is forced by actual wind observations obtained from the National Climatic Data Center, Ashville, N.C., TD-1129 data set. Wind observations are extracted from the raw data, and consist of marine surface wind observations originating from merchant ships, buoys, research vessels, and other ocean measurement stations, for the region 30°E - 122°E and 26°S - 26°N. Approximately 10 - 20 thousand observations are available per month.

The raw wind data are first converted to pseudostress by the following procedure, developed and discussed in detail by Legler, Navon and O'Brien (in preparation). Each observation's pseudostress value is initially calculated by:

$$|\vec{W}| = (u^2 + v^2)^{\frac{1}{2}} \tag{2a}$$

$$\tau_x = u|\vec{W}| \tag{2b}$$

$$\tau_y = v|\vec{W}| \tag{2c}$$

where u and v are the respective eastward and northward components of the wind. These pseudostress values are then filtered to remove wnere u and v are the respective eastward and northward components of the wind. These pseudostress values are then filtered to remove obviously erroneous reports, first by deleting any reports exceeding

40 ms^{-1}, and then by averaging all the τ_x and τ_y component values and deleting readings which fall outside upper (CH) and lower (CL) bounds defined as:

$$CH_x = \bar{\tau}_x + 30\,\bar{\tau}_x$$
$$CL_x = \bar{\tau}_x - 30\,\bar{\tau}_x$$
$$CH_y = \bar{\tau}_y + 30\,\bar{\tau}_y$$
$$CL_y = \bar{\tau}_y - 30\,\bar{\tau}_y$$

where $\bar{\tau}_x$, $\bar{\tau}_y$ are the average stress components in the north, east directions for the data and the value 30 was selected as a reasonably representative multiplicative factor upon which to establish acceptable ranges. The remaining reports are then binned into 1° latitude x 1° longitude blocks, and filtered a second time with respect to the standard deviation of all the reports in each individual block. Any report in a specific block exceeding ±3.7 standard deviations of its block value is deleted from the set, while the remaining values are retained to determine average pseudostress values for each block. Typically, less than 1% of the total reports are eliminated from the data set by these two filtering processes, but significant data gaps, generally located off standard shipping lanes, still exist. Filtered pseudostress charts for September - November 1985 are shown in Figs. 3 - 5. The remaining empty blocks in the filtered charts are assigned values through

September - November 1985 are shown in Figs. 3 - 5. The remaining empty blocks in the filtered charts are assigned values through

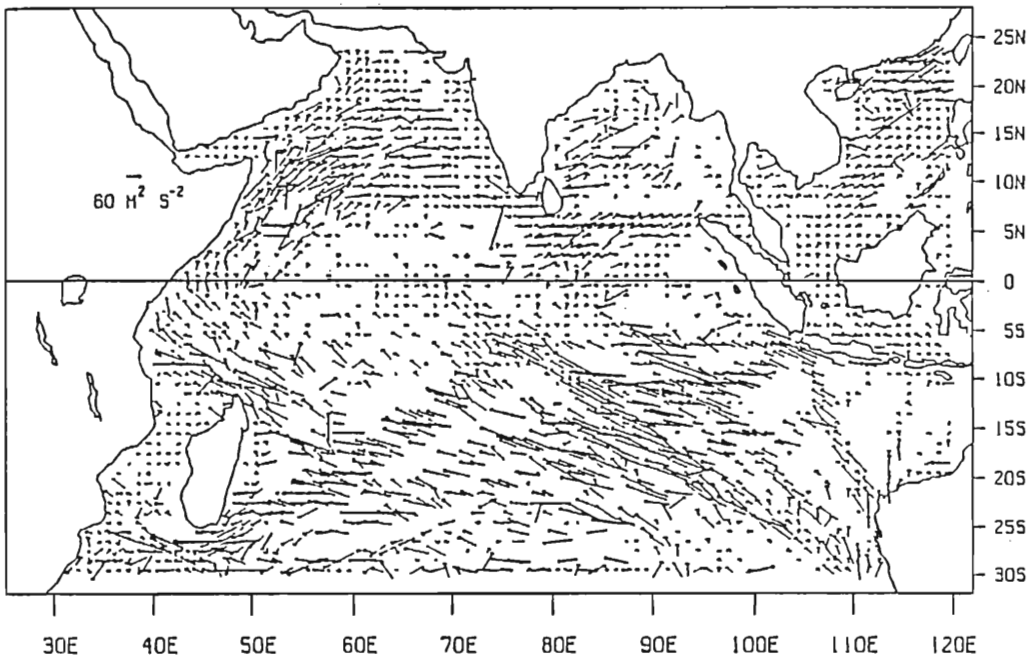

Fig. 3. Filtered pseudostress for September 1985. Arrows provide direction and magnitude with units of $m^2 s^{-2}$. The chart is derived from actual wind observations and has been filtered to remove obviously erroneous reports. Large gaps, generally located off standard shipping lanes exist, but the area around and north of Socotra is well covered. Note the region of high pseudostress around and to the southeast of Socotra.

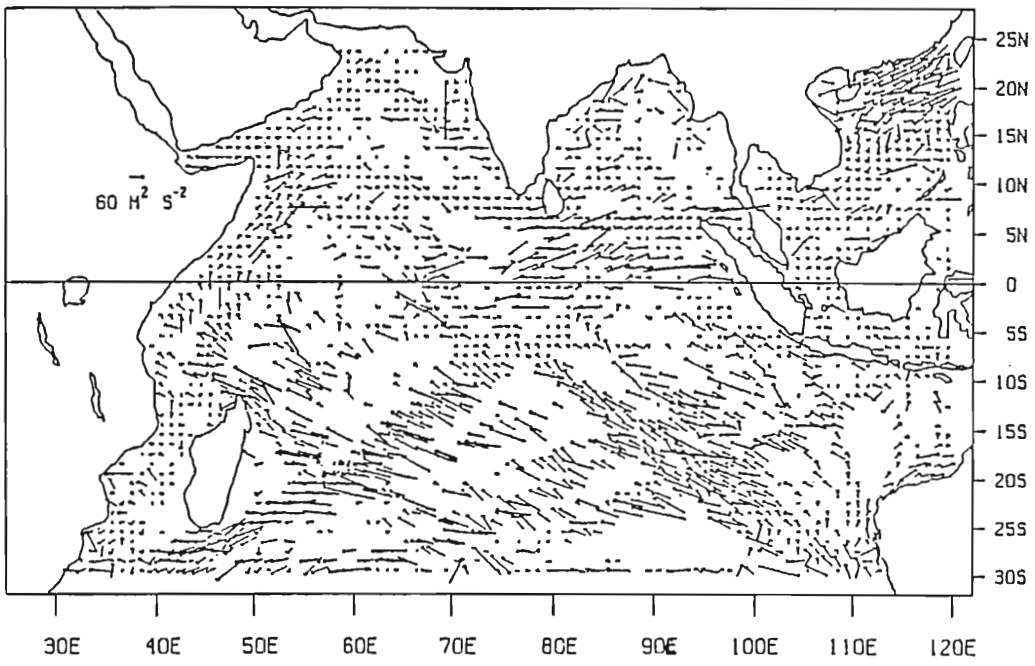

Fig. 4. Filtered pseudostress for October 1985. Same as fig. 3, except even larger gaps in the data exist. The region of high pseudostress off Somalia has weakened and retreated slightly to the southwest.

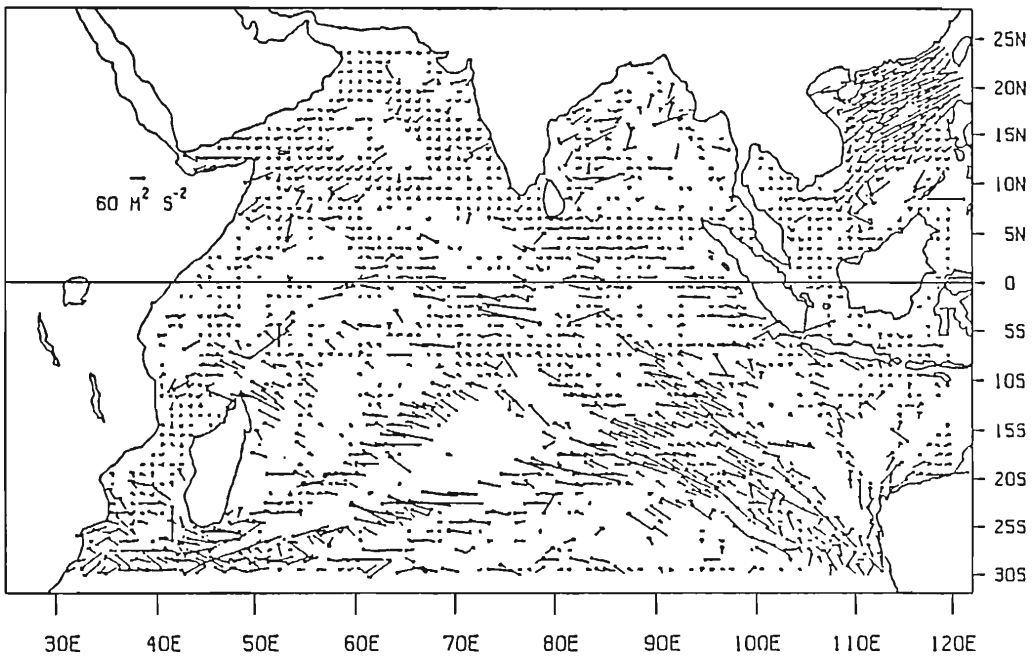

Fig. 5. Filtered pseudostress for November 1985. Same as fig. 4, but the direction of the pseudostress vectors has now shifted to the northeast, indicating the onset of the northeast monsoon.

bilinear interpolation, while grid points over land are assigned values by extrapolating the marine data, such that the gradient of the vector values normal to the coastal boundaries is zero.

The next step in the wind analysis involves the defining and minimizing a functional, F, which is used to calculate the final pseudostress values using the conjugate-gradient method:

$$F = \frac{1}{L^2} \sum_x \sum_y \left[(\tau_x - \tau_{x_o})^2 + (\tau_y - \tau_{y_o})^2 \right] +$$

$$+ \frac{\gamma}{L^2} \sum_x \sum_y \left[(\tau_x - \tau_{x_c})^2 + (\tau_y - \tau_{y_c})^2 \right]$$

$$+ L^2 \Gamma \sum_x \sum_y \left[\left(\nabla^2(\tau_x - \tau_{x_c})\right)^2 + \left(\nabla^2(\tau_y - \tau_{y_c})\right)^2 \right] \qquad (3)$$

$$+ \beta \sum_x \sum_y \left[\nabla \cdot (\vec{\tau} - \vec{\tau}_c) \right]^2$$

$$+ \alpha \sum_x \sum_y \left[\hat{k} \cdot \nabla \times (\vec{\tau} - \vec{\tau}_c) \right]^2$$

where τ_x, τ_y are the pseudostress values to be determined; τ_{x_o}, τ_{y_o} are the components of the filtered measured values; τ_{x_c}, τ_{y_c} are the components of pseudostress climatology obtained from Hellerman and Rosenstein (1983); $\vec{\tau}$, $\vec{\tau}_c$ are the determined and climatological pseudostress vectors; L is a length scale for dimensional consistency; and α, β, γ, and Γ are coefficients which are assigned values that weight the relative importance of each of the five terms of equation

and α, β, γ, and Γ are coefficients which are assigned values that weight the relative importance of each of the five terms of equation

(3) with respect to the other terms. Hence, the function, which is minimized after assigning values to the known parameters, calculates final pseudostress values that in a least squares sense are close to the filtered data values (1st term) and the climatological values (2nd term) for the region. Smoothing is performed in terms 3 - 5, with term 3 serving as a measure of the data roughness and controlling the "radius of influence" of a particular anomaly in the climatology or the input winds, and terms 4 and 5 serving as kinematic terms that force the divergence (term 4) and the curl (term 5) toward the kinematics of the climatology. The final pseudostress charts calculated for actual wind data from the fall of 1985 are shown in Figs. 6 - 8. For this study, these pseudostress fields were converted to wind stress by the bulk aerodynamic formula:

$$\vec{\tau} = \rho_a \vec{C}_D \vec{W} |\vec{W}|$$

where ρ_a is the density of air and C_D is a constant drag coefficient. For the results presented here, ρ_a = 1.2 kg m^{-3} and $C_D = 1.25 * 10^{-3}$. These values provide reasonable upper layer transports, consistant with a number of previously observed results, (eg. Leetmaa et al. (1982); Luther, et al. (1985)).

b) Corroborative Data

During the fall of 1985, U.S. Navy ships in the Arabian Sea collected XBT readings, while NOAA-8/9 spacecraft imaged the regions

During the fall of 1985, U.S. Navy ships in the Arabian Sea collected XBT readings, while NOAA-8/9 spacecraft imaged the regions

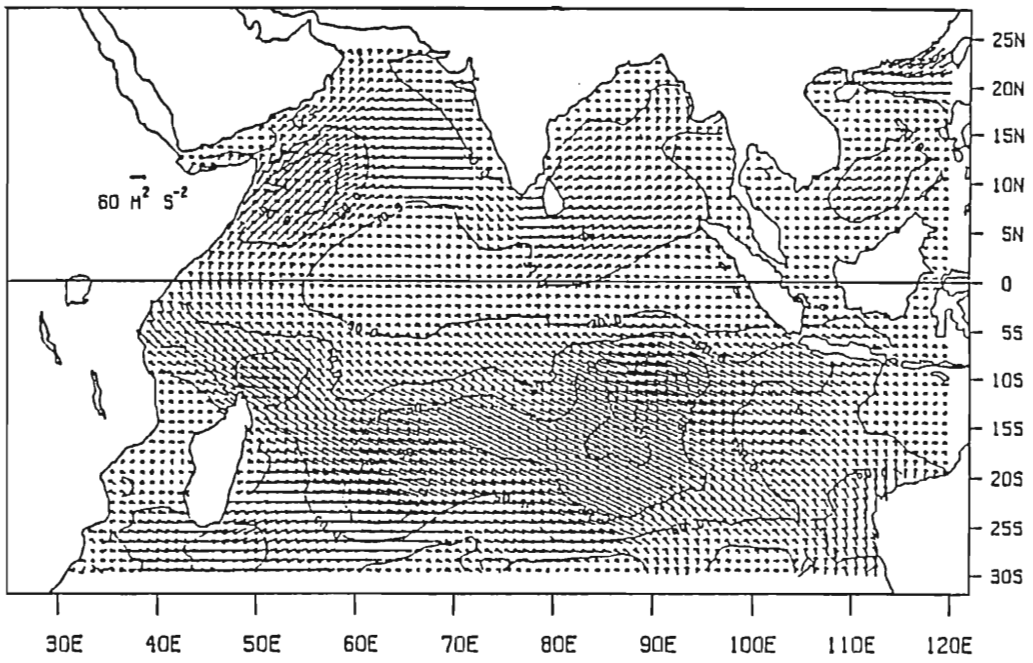

Fig. 6. Complete pseudostress for September 1985. These data are computed by bilinearly interpolating the filtered pseudostress data of fig. 3 to fill in empty regions, and then determining pseudostress values by the conjugate-gradient minimization process developed by Legler, Navon, and O'Brien. Arrows again provide direction and magnitude of the pseudostress in units $m^2 s^{-2}$. Contours provide a visual interpretation of regions of high and low pseudostress. Note the region of strong southwesterly pseudostress to the south-southeast of Socotra Island.

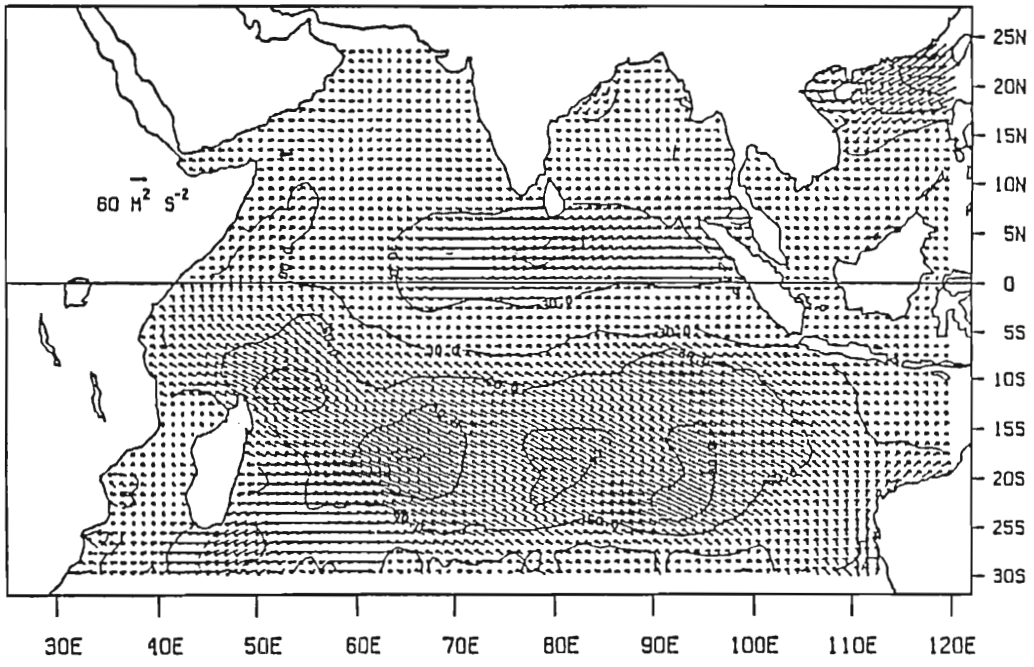

Fig. 7. Complete pseudostress for October 1985. Same as fig. 6. Values around and to the north of Socotra have diminished significantly, and direction reversal has begun.

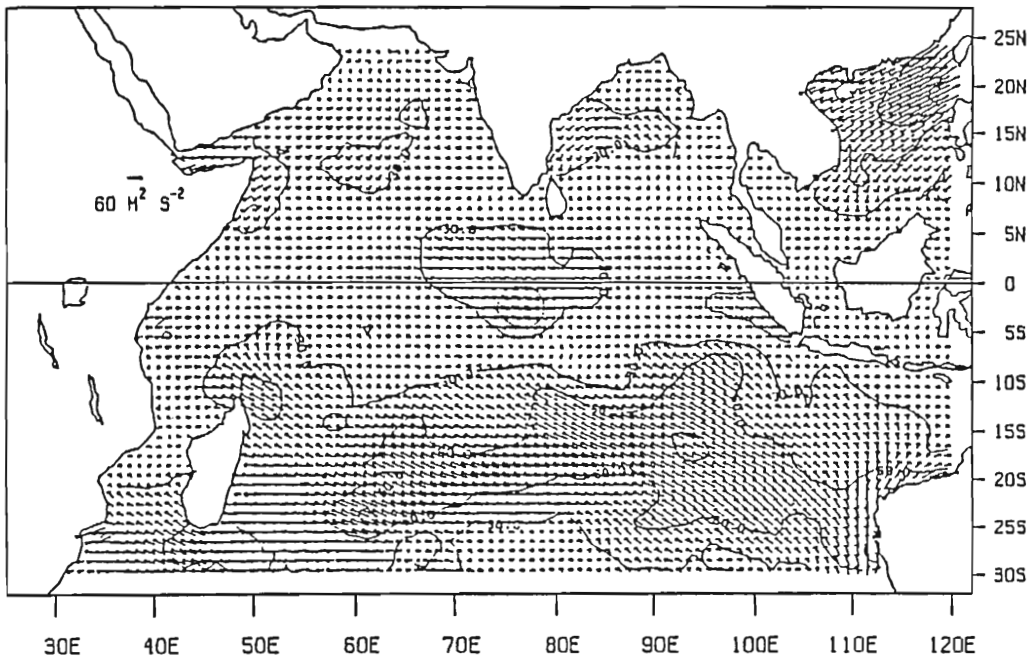

Fig. 8. Complete pseudostress for November 1985. Same as fig. 7. Direction has reversed north of the equator and maxima from the northeast begin to form to the east and southwest of Socotra.

surrounding Socotra Island and off the coast of the Arabian Peninsula. 353 BT readings and 20 AVHRR channel 4 satellite images were obtained for this study, covering the area from 8°N - 23°N and 50°E - 65°E. These data were analyzed to determine the actual oceanographic features present in the northwest Arabian Sea during September - November 1985. These features were then used to verify the accuracy of the fall 1985 model output resulting from the realistic wind data used to force the model.

BT data were received from the Navy in standard Navy message format, and were decoded to extract date, time, position, temperature, and depth information, which was then used to plot geographic positions and temperature vs depth profiles. Due to geographic limitations in the available data - approximately 150 of the 183 September BT readings were taken off the coast of Oman, while about 120 of the 170 October readings were taken around Socotra Island - two charts were developed, one bounding the region 13°N - 23°N and 58°E - 66°E, which contained the September BT readings, and the other bounding the region 8°N - 18°N and 50°E - 60°E, which contained the October BT readings. Temperature vs depth profiles were then used to determine an isotherm that provided a reasonably accurate representation of the thermocline depth for the two regions. The 20° isotherm was found to be most representative of the thermocline depth for the September data, while the 18° isotherm best represented the October thermocline depth. The readings were next separated into six

10-day increments extending from 1 - 10 September to 20 - 30 October, and each BT was plotted at its correct geographic position on the appropriate 10 day chart. The six charts were then depth contoured, based upon the 20°C (September) or 18°C (October) isotherm and dynamic oceanographic features extracted. Throughout this process the assumption was made that a shallow thermocline (and associated cooler water temperatures) was indicative of upwelling or upward Ekman pumping, while a deeper thermocline (and associated warmer water temperatures) was indicative of downwelling or downward Ekman pumping. The chart generated for 10 - 20 October is shown in Fig. 9.

Similarly, AVHRR satellite images of the Arabian Sea, obtained from the Scripps Satellite Oceanography Facility, covering the period 30 August - 30 November 1985, were analyzed to determine the oceanographic features present during September - November 1985. Due to the recording schedule for the satellites, nighttime channel 3 passes were unavailable during the time frame of this study and therefore only daytime channel 4 data, which is extremely susceptible to atmospheric moisture contamination, were collected. A number of the images were excessively contaminated by monsoonal moisture, but sufficient images were acceptable to determine many of the significant oceanographic features present during the period. A sample image from the NOAA-9 pass of 2 November 1985 is shown in Fig. 10.

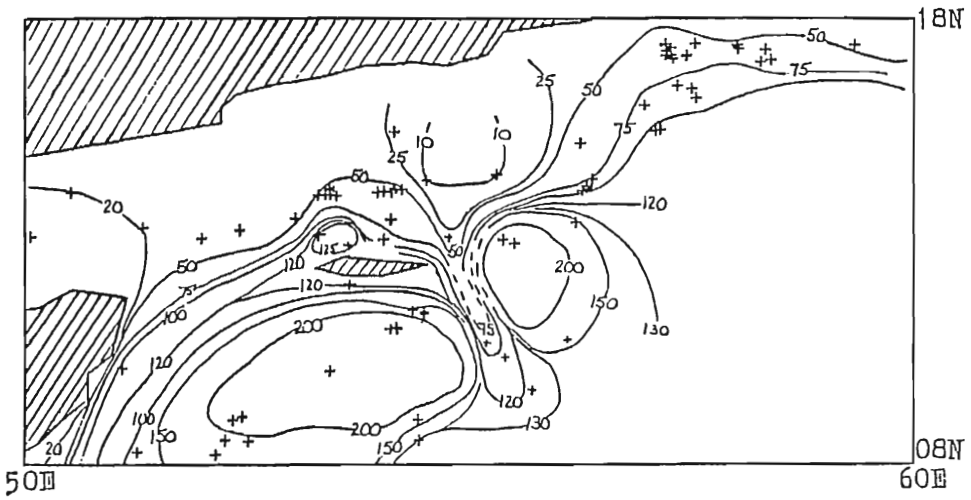

Fig. 9. The 18°C isotherm depth (meters) for 10 - 20 October 1985. Contours are generated from XBT data obtained by the U.S. Navy over the ten day period, for which depth profiles indicated that the 18°C isotherm best represented the thermocline depth. Dashed lines indicate regions of deficient BT readings and are estimated contours. Three anticyclonic eddies appear to the south, east and northwest of Socotra and a cyclonic eddy appears to the northeast, with an attached tongue of cool water penetrating to the south along the eastern shore of Socotra. Strong fronts appear off the Somali coast and between the four dominant eddies.

Fig. 10. NOAA-9 AVHRR image of 2 November 1985 for the region between Socotra Island and the Arabian Peninsula. Socotra is located at the bottom center of the image, while Yemen extends along the top. Warm surface temperature, indicative of anticyclonic flow can be recognized by the lightly shaded region north and northwest of Socotra, while cooler water, incicated by the darker shading, is observed in the upper center of the image, south of and offshore of the Arabian Peninsula between Ras Fartak and Ras Marbat.

RESULTS

a) Preface

The emphasis of this study is focused on the transition period between the breakdown of the southwest monsoon and the spin-up of the northeast monsoon during September - November 1985 for the northwest Arabian Sea, around and north of Socotra Island. Fig. 11, the 16 October 1985 model output, introduces the dynamic features discussed throughout the study. Three anticyclonic eddies - the great whirl, south of Socotra; Socotra Eddy, east of Socotra; and the North Socotra Warm Eddy, north and northwest of Socotra - and one cyclonic eddy - the North Socotra Cyclonic Eddy, northeast of Socotra - dominate the dynamic features around Socotra Island, while to the north, along the Arabian Peninsula, a large relatively homogeneous thin upper layer structure extends from immediately along the coast to well offshore. For results presented here, the following assumptions are made:

- a thin upper layer thickness (ULT) in the model indicates upwelling or prior Ekman suction, while a thick ULT indicates downwelling or prior pumping.
- a thin layer in the BT data, corresponding to a shallow thermocline, is indicative of upwelling or prior Ekman suction, while a deep BT thermocline is indicative of downwelling or prior Ekman pumping.
suction, while a deep BT thermocline is indicative of downwelling or prior Ekman pumping.
- cool satellite sea surface temperature (SST) is indicative of

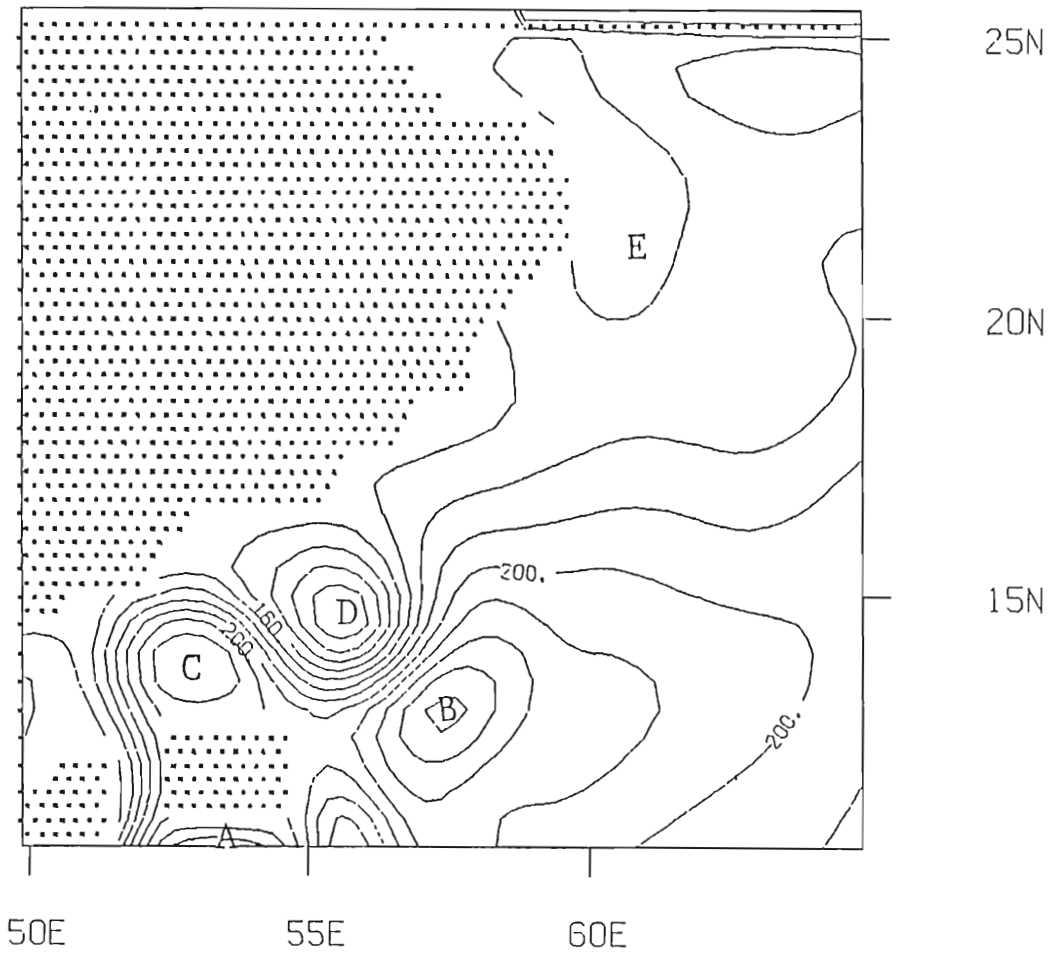

Fig. 11. Model response (ULT) for 16 October 1985 forced by observed winds. Four prominent eddies appear around Socotra Island - the anticyclonic great whirl to the south (A); Socotra Eddy to the east (B); and North Socotra Warm Eddy to the northwest (C), and the cyclonic North Socotra Cyclonic Eddy to the northeast (D). Further north, a large homogeneous region of relatively constant ULT exists off the coast of Oman (E). Contour interval is 10 meters.

cyclonic North Socotra Cyclonic Eddy to the northeast (D). Further north, a large homogeneous region of relatively constant ULT exists off the coast of Oman (E). Contour interval is 10 meters.

upwelling or prior Ekman suction, while warm SST is indicative of downwelling or prior Ekman pumping.

b) 1985 Response to Observed Wind Forcing

The 1985 model response to observed wind forcing, generated by obtaining a steady seasonal cycle in the model, and then repeatedly applying the observed 1985 monthly mean winds to the model for four years, demonstrates an expected oceanographic seasonal response to the shifting monsoonal winds. Focusing on the region from 8°N - 23°N and 50°E - 65°E, the oceanic response at the beginning of the year (January - March) reflects a general breakdown of the dynamic flow pattern established in the previous year. The Socotra Eddy migrates slowly westward and weakens as it gradually coalesces with the North Socotra Warm Eddy. Closed circulation in the North Socotra Cyclonic Eddy breaks down and a thick ULT from along the Arabian coast fills the area vacated by the westward migrating Socotra Eddy. The great whirl, south of Socotra, relaxes, while a thicker ULT fills the entire region off the Omani Coast.

During the spring, as the Southeast trade winds begin to intensify to the north and penetrate the Socotra region, the 1985 dynamic response begins to develop. From the Indian Ocean interior, Rossby waves approach from the east, while the previous year's Socotra and North Socotra Warm Eddies coalesce, maintain a slow westward drift, and continue to weaken. The North Socotra Cyclonic Eddy reintensifies, but its center shifts to the northwest during April.

drift, and continue to weaken. The North Socotra Cyclonic Eddy reintensifies, but its center shifts to the northwest during April.

Remnants of the great whirl continue to weaken south of Socotra, while to the north, ULT throughout the region slowly begins to thin again. During the summer, with the southwest monsoon now fully developed, the dominant fall eddies begin development. From early June to about 11 August, the previous year's coalesced Socotra and North Socotra Warm Eddies continue to weaken and finally breakdown. Corrrespondingly, the upper layer of the entire region between Socotra and the Arabian Peninsula thins. By 18 August, flow from around the western end of Socotra intensifies, thickening the ULT of the region and stimulating development of the 1985 North Socotra Warm Eddy. This flow rapidly closes off anticyclonically, shifts to the east, and further intensifies. The North Socotra Cyclonic Eddy expands to the southeast in early July and intensifies throughout the summer. By the end of August, the eddy has become quite strong and a tongue of thin ULT extends from the south of the eddy along the eastern shore of Socotra Island. Further to the east, Rossby waves continue to penetrate from the ocean interior, but are blocked by Socotra and the now strong North Socotra Cyclonic Eddy. The Rossby waves pile up and thicken the ULT east of Socotra, and by 5 September, anticyclonic flow, indicating the development of the 1985 Socotra Eddy, appears at about 62°E. The 1985 great whirl, migrating from the south, makes its first appearance off the southern coast of Socotra on 15 July and abuts the island by 1 August. Rapid intensification of the anticyclonic flow occurs from 10 August - 13 September as the center of the eddy further penetrates to August. Rapid intensification of the anticyclonic flow occurs from 10 August - 13 September as the center of the eddy further penetrates to

the north. Off the Omani coast, a slow but constant thinning of the ULT occurs over the entire region until 23 August, when the flow reverses and a thickening of the ULT begins to the north, immediately off the coast of Rás al Haad.

During the fall, the great whirl, Socotra Eddy, and North Socotra Warm Eddy establish themselves to the south, east, and northwest of Socotra Island. The North Socotra Cyclonic Eddy is present to the northeast of Socotra, with a tongue of thin ULT extending to the south along the eastern shore of the island. This provides a region of frontal separation between both the Socotra Eddy and great whirl and the Socotra Eddy and Socotra Island itself. In November, the Socotra Eddy presses westward and closes off the thin ULT tongue, as the thicker ULT of the eddy penetrates to the coast of the island. Along the Omani coast to the north, thin ULT persists until mid-October when flow penetrating from the north thickens the ULT immediately along the coast of Oman, separating the large region of thin ULT from the Arabian Peninsula.

c) Eddy Formation

The study has revealed that the four principle eddies discussed above dominate the upper layer circulation around Socotra in the fall of 1985, and that the formation of these eddies is the result of four distinct mechanisms (Fig. 12). In the early stages of the southwest monsoon, the great whirl forms in response to the strong gradient in the curl of the core of the Findlater jet as it departs the African

monsoon, the great whirl forms in response to the strong gradient in the curl of the core of the Findlater jet as it departs the African

Fig. 12. Model results every 10 days from 1 August to 21 October 1985, chronologically displayed left-to-right, top-to-bottom. Clearly seen in the sequence are the formation mechanisms for three of the principle eddies observed around Socotra in the fall of 1985. The North Socotra Cyclonic Eddy (blue) is seen to the northeast of the island. It has formed from baroclinic instability in the Somali Current and is intensifying throughout the period. As the eddy strengthens and shifts southward, extending from the Arabian Peninsula to the eastern tip of Socotra, it becomes a contributing factor in the formation of the Socotra Eddy. Rossby waves, seen penetrating into the region from the southeast, are blocked by the intensified North Socotra Cyclonic Eddy. The waves build east of Socotra (thickening of the ULT) and by the beginning of October the circulation closes off anticyclonically, forming the Socotra Eddy. The eddy intensifies rapidly, thickens the ULT (red) and drifts westward toward Socotra. To the northwest, anticyclonic vorticity, introduced by the Somali Current as it flows west of Socotra, enters the mouth of the Gulf of Aden. The flow passes to the north of Socotra, turns eastward, and closes off anticyclonically into the North Socotra Warm Eddy (steadily thickening ULT). As with the other eddies, it also intensifies throughout the period. South of the island in September, the thick ULT of the great whirl can be seen, as it has migrated from its formation position at about 8°N to just south of Socotra.

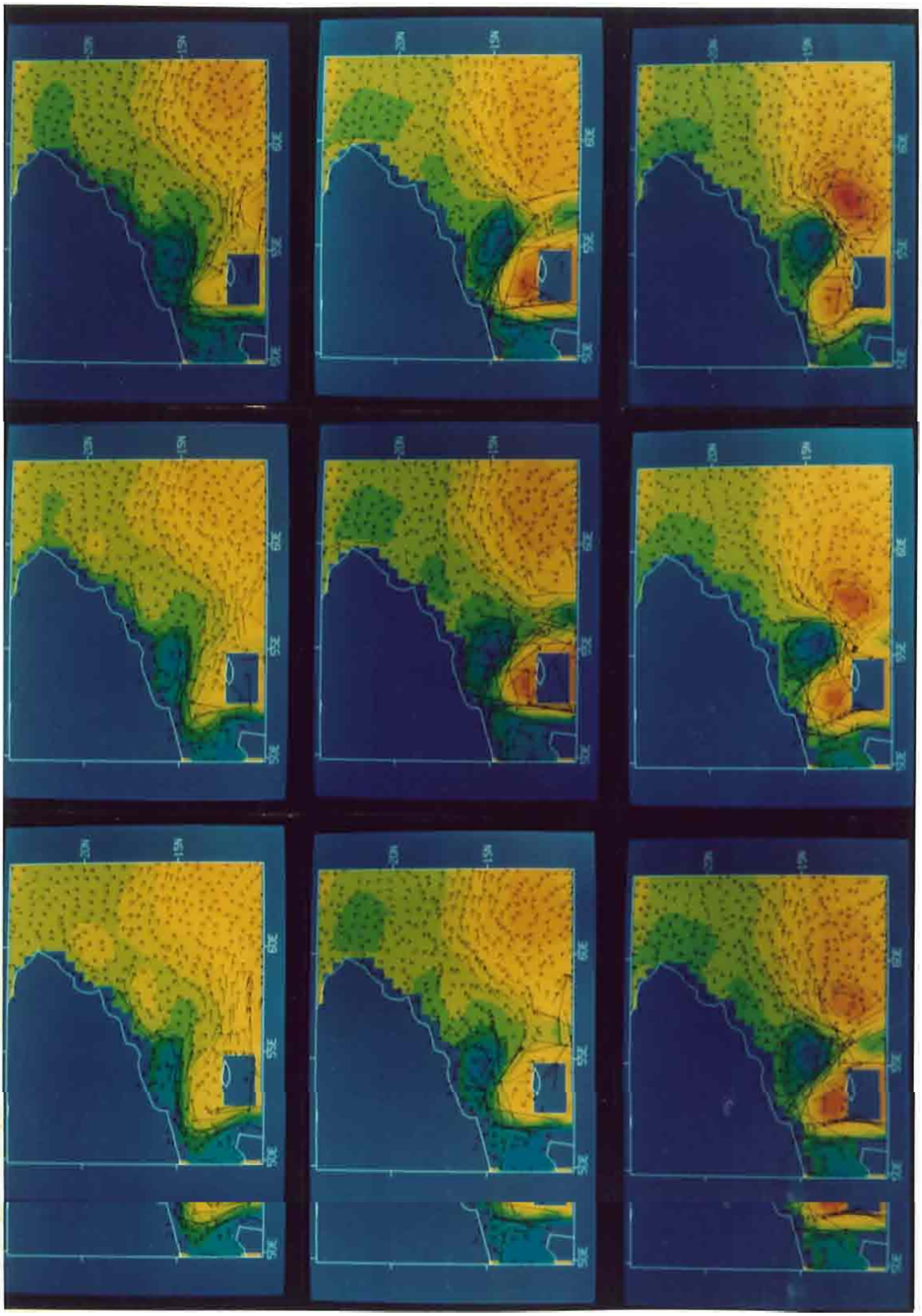

coast at about 8°N. It migrates northward in late August, as the winds retreat to the south, and appears south of Socotra in September.

The North Socotra Cyclonic Eddy is the most persistant of the eddies and is present during most of the year. Resulting from barotropic instability in the Somali Current, the eddy is very weak in the winter during the northeast monsoon, but in March, as the winds shift to the southwest, the eddy intensifies. It remains strong until June, when the northeast Somali Current penetrates the region and overruns the cyclonic flow. In late summer, as the Southeast trade winds retreat from the region and the upper layer current weakens, the eddy reintensifies, becoming quite strong between Socotra Island and the Arabian Peninsula. This positioning is important as it is significant in the formation of the anticyclonic Socotra Eddy, which results from Rossby waves that approach the Socotra region from the interior of the Indian Ocean.

In spring and early summer, Rossby waves pass through this region unimpeded, alternately deepening and thinning the upper layer. In late summer with the North Socotra Cyclonic Eddy well established between Socotra and the Arabian Peninsula, the Rossby waves are no longer able to pass through the region and they pile up east of Socotra, deepening the ULT, and closing off the flow anti-cyclonically. The result is the Socotra Eddy which forms east of the island.

Later in the southwest monsoon cycle, the North Socotra Warm Eddy island.

Later in the southwest monsoon cycle, the North Socotra Warm Eddy

forms to the northwest of Socotra. As the northeast Somali Current penetrates northward toward Socotra, the flow is forced to split south of the island. The portion that flows to the west of Socotra passes through the straits between Socotra and Somalia and, as it enters into the mouth of the Gulf of Aden, its anticyclonic vorticity circulates back around to the east, closing and forming the North Socotra Warm Eddy. The eddy is highly dependent upon this anticyclonic vorticity for energy and as a result, the eddy weakens considerably during November as the winds and current diminish and finally reverse. This is also a likely explanation for the absence of the North Socotra Warm Eddy in years of weak monsoon winds, as the much weaker northeast Somali Current is unable to provide sufficient anticyclonic vorticity to stimulate formation of the eddy.

d) Climatological Assessment

To determine the oceanographic dynamic structure for 1985 with respect to a "normal" or relatively consistent year for this region, two additional model cases were considered; one forced by observed winds analyzed by Cadet and Diehl (1984) from the period 1954 - 1976, and the other by monthly mean climatological winds from the same 23-year period. These results were then compared to the 1985 results forced by observed winds, to determine the unique features, if any, present in 1985.

Although no two years display the exact same structure, the observed wind 23-year case resulted in two reasonably consistent

Although no two years display the exact same structure, the observed wind 23-year case resulted in two reasonably consistent

patterns that frequently appeared. One, in which the great whirl, Socotra Eddy and North Socotra Warm Eddy appear, occurred in 13 of the 23 years ('54, '56, '58, '61-'68, '71, '72), while the other, in which the North Socotra Warm Eddy was absent from the system, occurred in the remaining 10 years ('55, '57, '59, '60, '69, '70, '73-'76). The two years, 1954, a year of relatively strong monsoon winds, and 1973, a year of relatively weak monsoon winds, are most representative of the two patterns, and are shown in Figs. 13 and 14. The climatological wind case is also shown, Fig. 15.

Comparison of these three cases with the 1985 case reveals that 1985 was, in fact, a relatively unique year. The well developed Socotra Eddy in September, cold tongue east of Socotra Island in October, and the absence of the two anticyclonic flows along 61°E for the entire period are all significant deviations from what is normally observed in the model. Fig. 16, a profile of the 1985 case and climatological case for 16 October across 14°N, graphically demonstrates the departure of the 1985 dynamics from the climatological response. Hence, 1985 did indeed provide a unique opportunity to assess dynamic features relatively uncommon in the region.

e) Model Assessment

Late August and early September marks the beginning of the active eddy development observed in the fall around Socotra Island and further to the north along the coast of the Arabian Peninsula. To the

eddy development observed in the fall around Socotra Island and further to the north along the coast of the Arabian Peninsula. To the

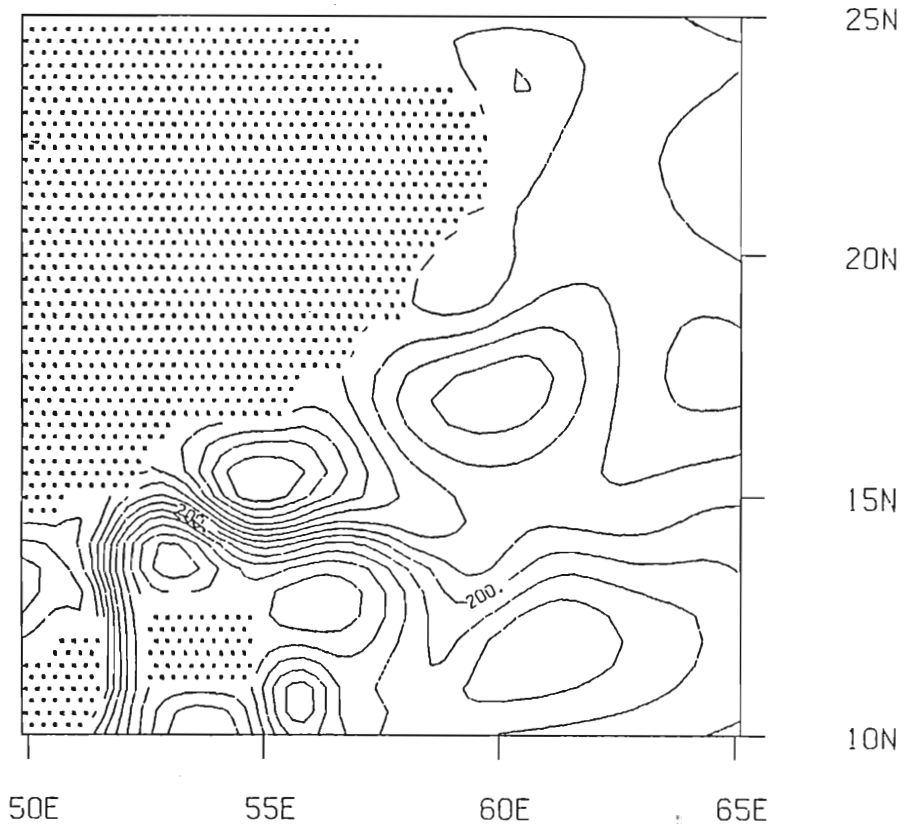

Fig. 13. Model response for 16 October 1954 forced by observed winds. Respresentative of a year of strong monsoon winds in which the three major anticyclonic eddies appear around Socotra, the great whirl, Socotra Eddy, and North Socotra Warm Eddy are present, but two additional anticyclone eddies occur along 60°E - one at 12°N and the other at 17°N. The North Socotra Cyclonic Eddy is present, but no cold tongue exists east of Socotra. Instead, a cyclonic eddy has formed to the southeast of the island. Along the Arabian Peninsula, a deeper layer penetrates from the south immediately off the coast, with a thinner layer extending offshore to about 62°E.

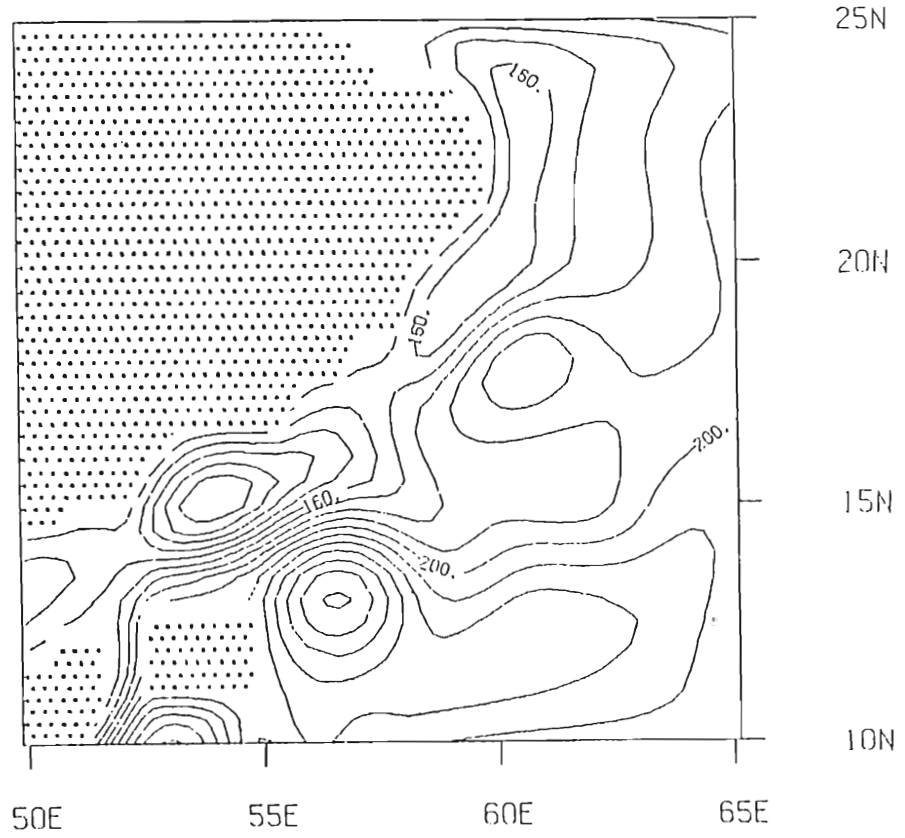

Fig. 14. Model response for 16 October 1973 forced by observed winds. Representative of a year in which monsoon winds were anomalously weak and only two of the major anticyclonic eddies occur around Socotra, the great whirl and Socotra Eddy appear, but the North Socotra Warm Eddy is absent. Again, two additional anticyclonic eddies are present along 61°E at 12°N and 17°N. The North Socotra Cyclonic Eddy extends all along the Arabian Peninsula, with a deep layer immediately along the Omani coast, and a thin layer extending to 62°E.

eddies are present along 61°E at 12°N and 17°N. The North Socotra Cyclonic Eddy extends all along the Arabian Peninsula, with a deep layer immediately along the Omani coast, and a thin layer extending to 62°E.

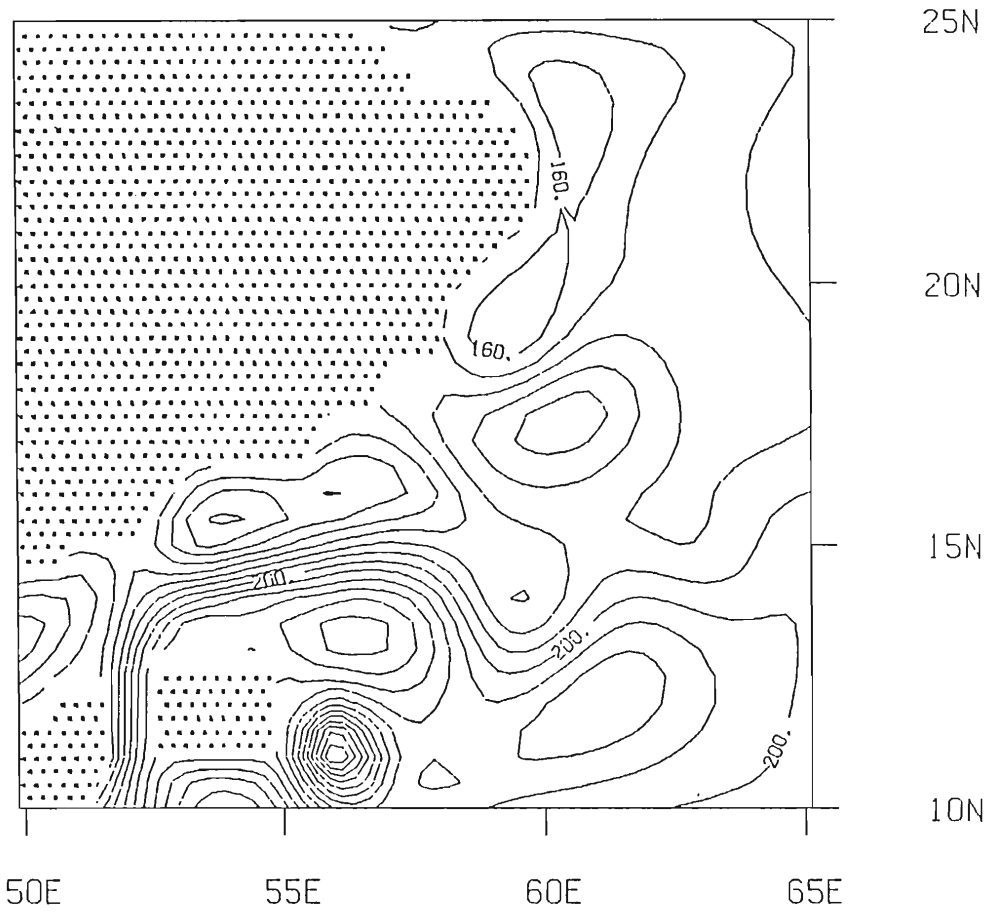

Fig. 15. Model response for 16 October forced by climatological winds. Five anticyclonic eddies occur: the great whirl, Socotra Eddy, a weak North Socotra Warm Eddy, and two along 61°E at 12°N and 17°N. Cyclonic eddies, in addition to the North Socotra Cyclonic Eddy along the Arabian Peninsula, occur southeast of Socotra and along 60°E at about 14°N, 19°N, and 23°N. A deep layer penetrates from the north immediately off the Omani coast with a thin layer extending to about 63°E.

immediately off the Omani coast with a thin layer extending to about 63°E.

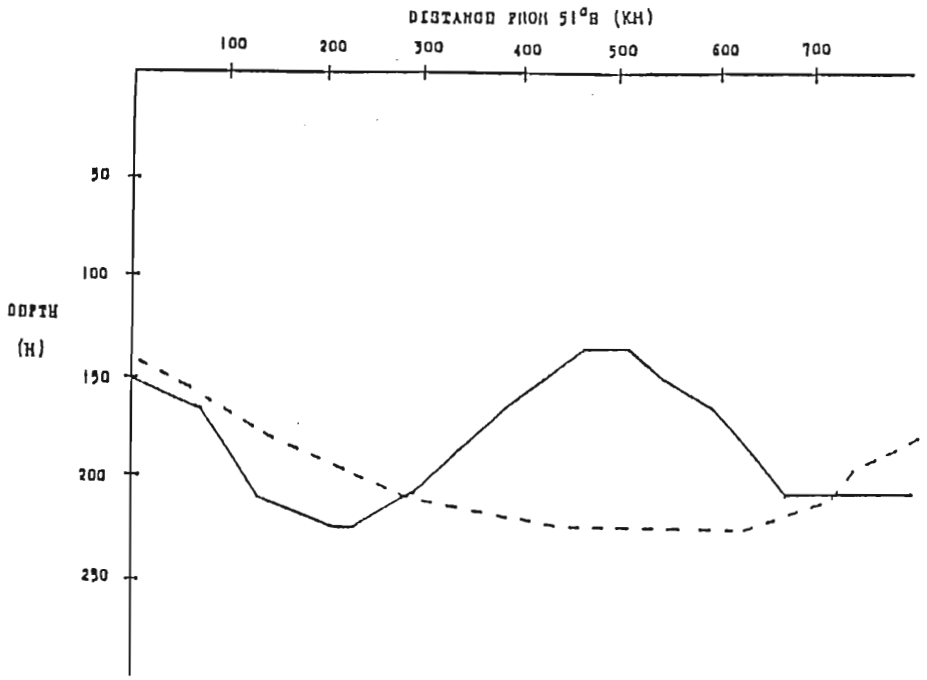

Fig. 16. Upper layer profiles for the case forced by 1985 observed winds (solid line) and the case forced by climatological winds (dashed line) for 16 October 1985, along 14°N. Distances are measured east from 51°E. The North Socotra Warm Eddy at about 220km, and Socotra Eddy at about 680km, are distinctly separated by the North Socotra Cyclonic Eddy at about 480km in the 1985 case. In the climatological case, the two anticyclonic eddies have coalesced into one large eddy with maximum depth attained at about 500-600km, indicating that in 1985 the North Socotra Cyclonic Eddy was located well south of its climatological position.

south, at the beginning of September, formation of the North Socotra Warm Eddy dominates the dynamics around Socotra. Closed anticyclonic flow, with its associated thick ULT, is observed to the northwest of the island, while a region of thin ULT extends south from the Arabian Peninsula along and to the northeast of the island (Fig. 17). Figs. 18 and 19, a NOAA-8 SST satellite image for 30 August, confirm the presence of warmer water of the North Socotra Warm Eddy along the northwestern edge of Socotra and cooler water located to the northeast. In figs. 20 and 21, it can be seen from profiles along 14°N and 15°N of satellite SST and model response for 1 September, that these two distinct features are properly positioned by the model.

Along the coast of the Arabian Peninsula, a large relatively homogeneous region of constant ULT exists, extending eastward to about 65°E. This feature, along with a pocket of thick ULT at about 20°N, is present in the region in mid-September, and appears in both the model response and the BT readings of 16 September (Figs. 22 and 23). A profile comparison along 21°N for this date (Fig. 24), shows the warm region off the coast, followed by the large region of thin ULT and cooler water further to the east. A feature noticeably absent from the model, however, is the region of upwelling that extends approximately 50 - 60 km immediately off the coast in the BT data. This failure of the model to predict the thin zone of coastal upwelling along the Omani coast occurs throughout September in the model results and appears to be a deficiency in the model.

upwelling along the Omani coast occurs throughout September in the model results and appears to be a deficiency in the model.

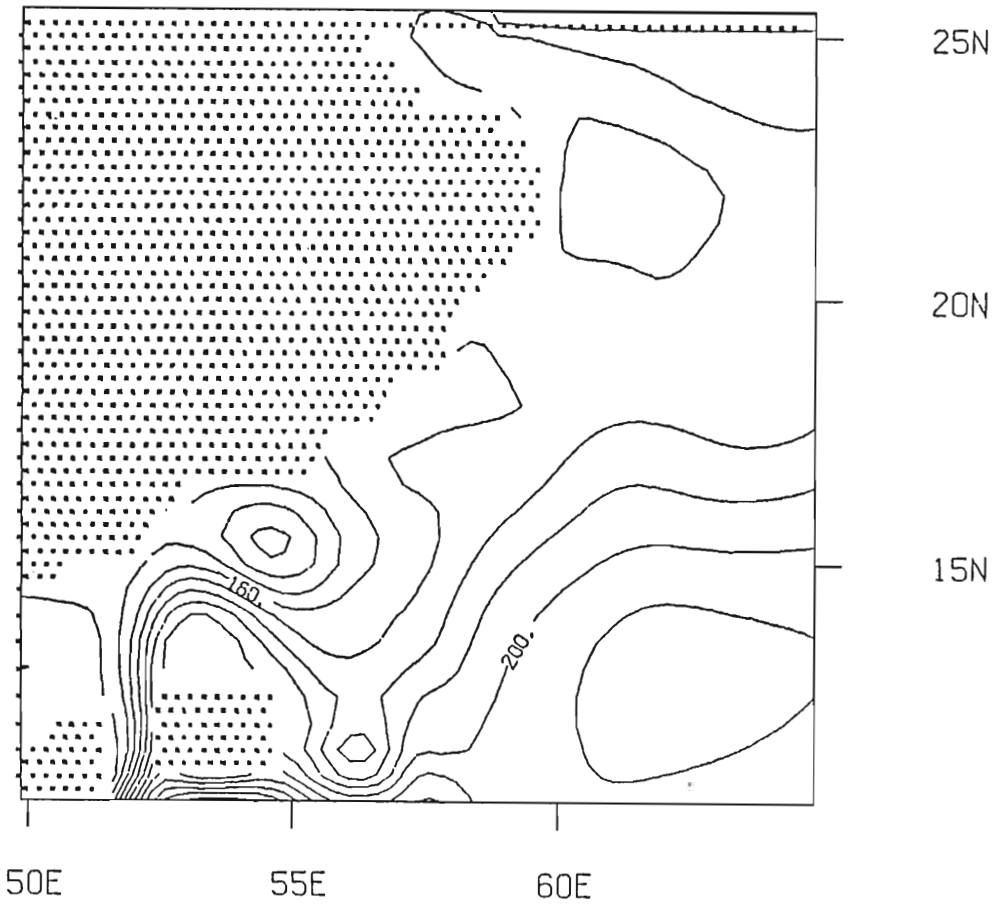

Fig. 17. Model response for 1 September 1985. The North Socotra Warm Eddy is well established to the north-northwest of Socotra Island, while a large homogeneous region of thinner ULT (cooler water) stretches along the coast of the Arabian Peninsula. A tongue of thin ULT penetrates down the eastern shore of Socotra, while early formation of the Socotra Eddy is observed further to the east, at about 58°E.

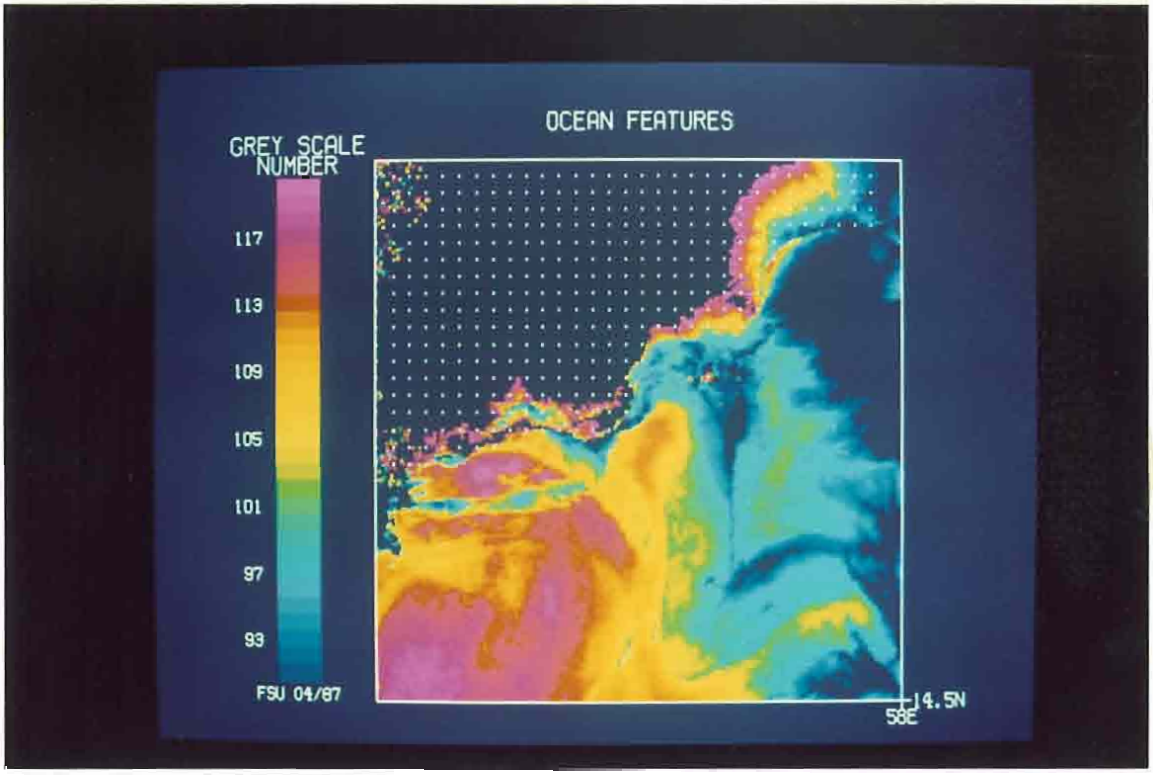

Fig. 18. The northwest quadrant of the NOAA-8 AVHRR image of 30 August 1985 for the region south of the Yemen coast. The reference position, 14.5°N/58°E, is located in the lower righthand corner of the image. The light blue region along the eastern third of the image indicates cooler sea surface temperatures, indicative of the North Socotra Cyclonic Eddy, while the yellow and purple region to the west, indicates warm surface temperatures, indicative of the North Socotra Warm Eddy.

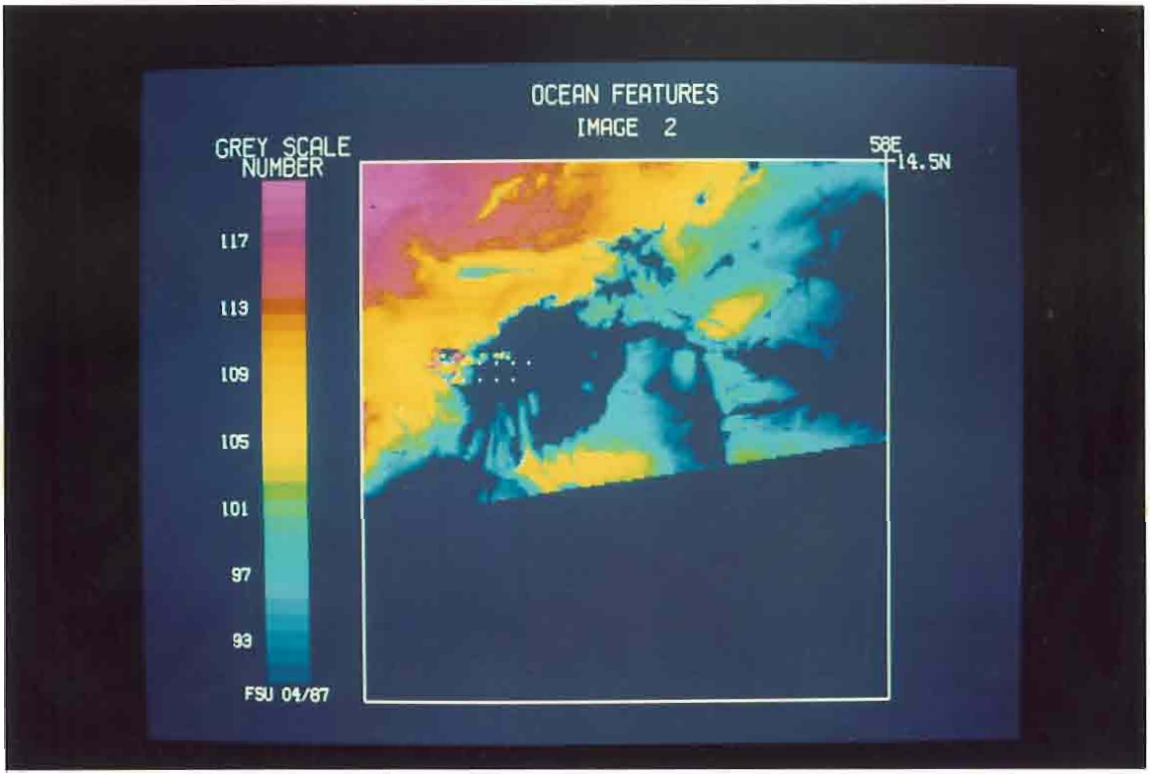

Fig. 19. The southwest quadrant of the NOAA-8 AVHRR image of 30 August 1985 for the region surrounding Socotra Island, indicated by the dotted outline in the left-center of the image. 14.5°N/58°E is located in the upper righthand corner of the image. The light blue region east of Socotra indicates cooler sea surface temperatures, while the yellow and purple region in the upper left indicates warmer surface temperatures, indicative of the North Socotra Warm Eddy.

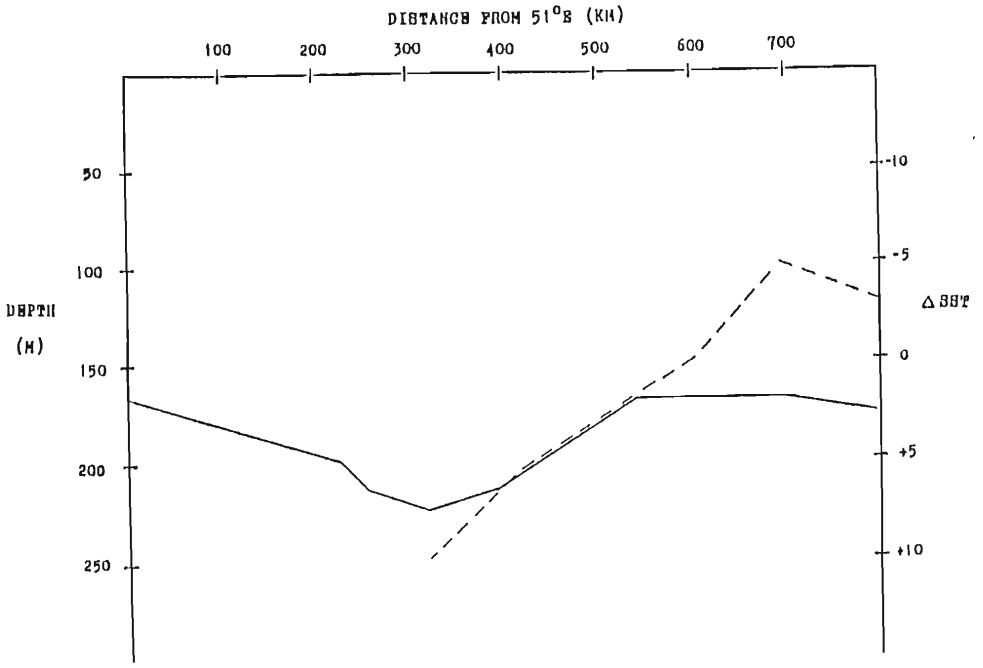

Fig. 20. Profiles of the sea surface temperature anomalies from the NOAA-8 AVHRR image of 30 August 1985 (dashed line) and the model ULT for 1 September 1985 (solid line) along 14°N. Distances are measured east from 51°E, with AVHRR data available between 300 km and 800 km. The cold tongue extending south from the North Socotra Cyclonic Eddy is apparent in both profiles between 600km and 700km. Likewise, the North Socotra Warm Eddy is apparent in each, with a maximum depth at about 300km.

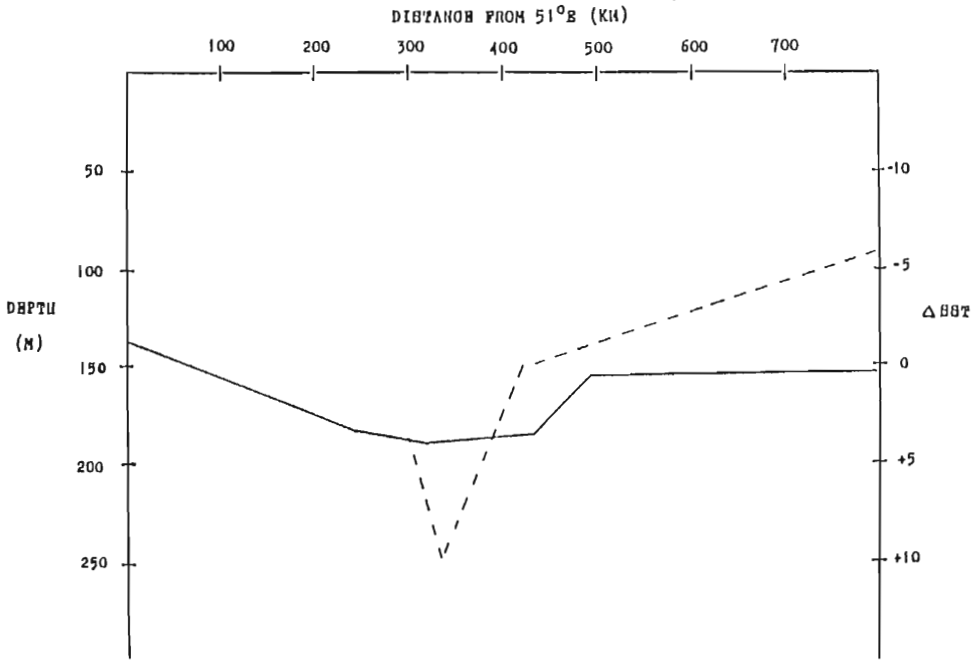

Fig. 21. Same as fig. 20, along 15°N. Again, the North Socotra Warm Eddy appears properly placed by the model, reaching a maximum at about 320km.

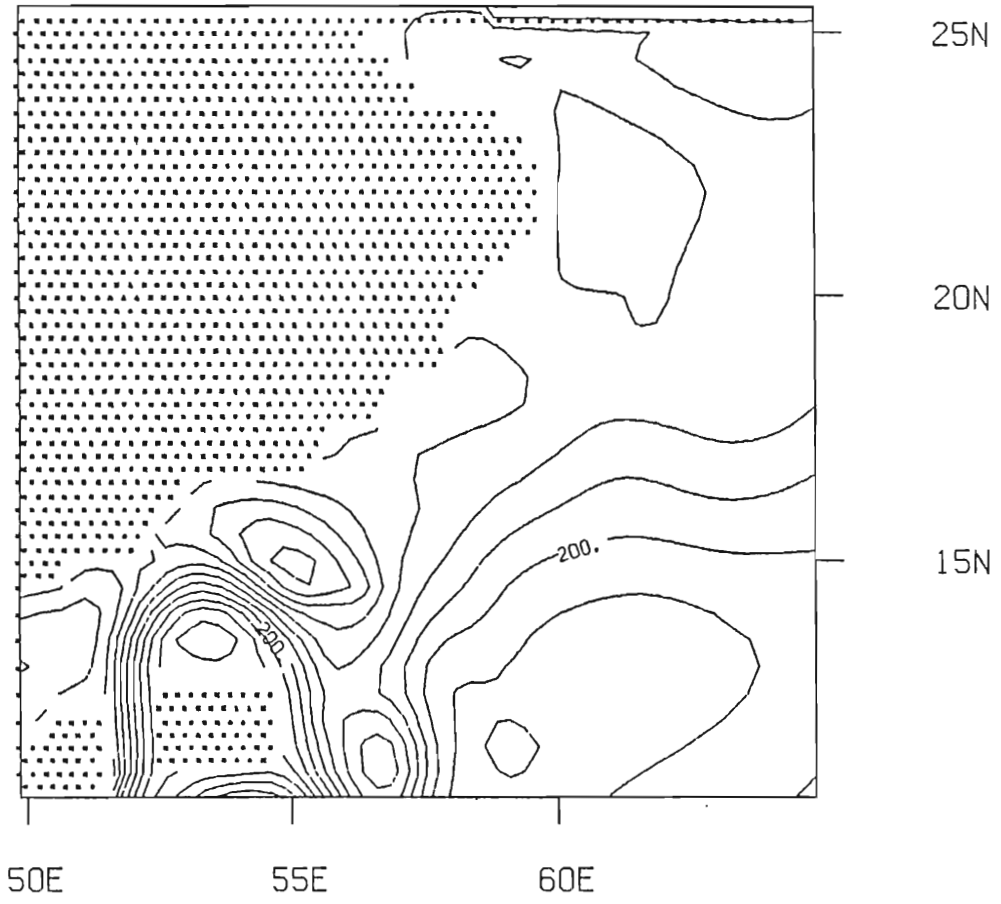

Fig. 22. Model response for 16 September 1985. The great whirl, south of Socotra Island, and the North Socotra Warm Eddy, north of Socotra, are well established. The North Socotra Cyclonic Eddy, with a thin layered (cool) tongue extending south from it, is intensifying northeast of Socotra, while indications of the Socotra Eddy formation appear east of Socotra at about 58°E. To the north, off Oman, a deep layered (warm) tongue of water separates a large pocket of thinner layer (cooler) water from the coast.

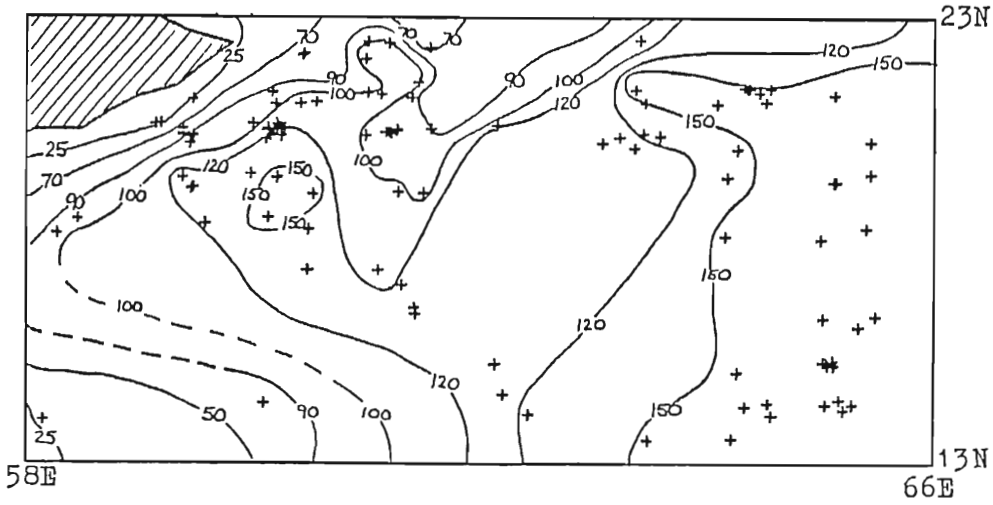

Fig. 23. The 20°C isotherm depth (meters) for 10 - 20 September 1985. Dashed lines indicate regions where BT data is deficient and contours are estimated. Upwelling persists off the Omani coast, with thermocline deepening (warming) increasing with distance from shore. A shallow (cool) tongue penetrates from the north at about 19°N between 61°E and 62°E, while indications of a small anticyclonic eddy appear centered at about 19°N/60.5°E.

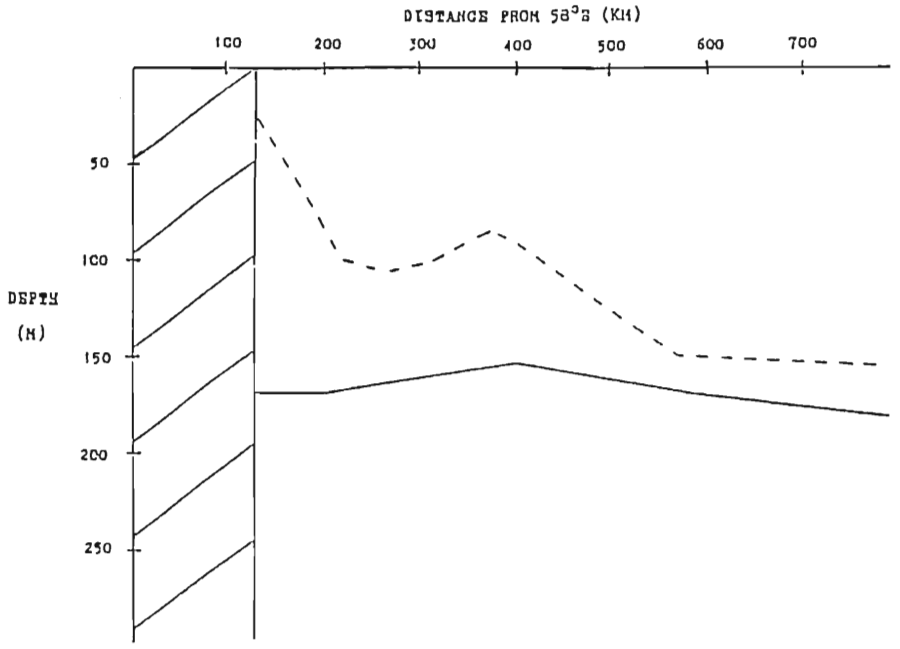

Fig. 24. Profiles of the BT 20°C isotherm depth for 10 - 20 September 1985 (dashed line) and model ULT for 16 September 1985 (solid line). Distances are measured east from 58°E, along 21°N, with the coast of the Arabian Peninsula extending over the first 130km. Both profiles show the relatively homogeneous pocket of water extending out beyond 800km, with a thin (cool) region appearing at about 380km. The BT data clearly shows a 50 - 60km region of upwelling immediately off the coast of Oman, which is absent from the model response.

Throughout the remainder of September, the region off the Omani coast (for which the majority of September BT data exist) remains relatively constant in structure in both the model and the BT data. Again, the data clearly displays an upwelling region immediately off the coast, which is absent from the model. To the south, around Socotra, BT data is insufficient to distinguish dynamic features, but the model shows an intensification of the North Socotra Warm Eddy and the formation of the North Socotra Cyclonic and Socotra Eddies, in what are their reasonably expected positions.

As seen in Fig. 11, the model shows October to be the most dynamically active month for the region surrounding Socotra. The remnants of the great whirl to the south, North Socotra Warm Eddy to the northwest, North Socotra Cyclonic Eddy to the northeast, and Socotra Eddy to the east, all display very active patterns and provide numerous flow and frontal characteristics upon which a comparison of the model and the available BT and satellite data can be conducted.

The BT data for 1 - 10 October, contoured in Fig. 25, shows the great whirl, Socotra Eddy and North Socotra Cyclonic Eddy, as well as an indication of the North Socotra Warm Eddy which in fact is present, as satellite imagery for this period confirms. Significantly, it also shows the thin ULT tongue extending south from the North Socotra Cyclonic Eddy along the eastern shore of Socotra. As previously discussed, this is a unique feature of 1985, and is clearly present in the model result for 6 October, shown in Fig. 26. Profiles of these

discussed, this is a unique feature of 1985, and is clearly present in the model result for 6 October, shown in Fig. 26. Profiles of these

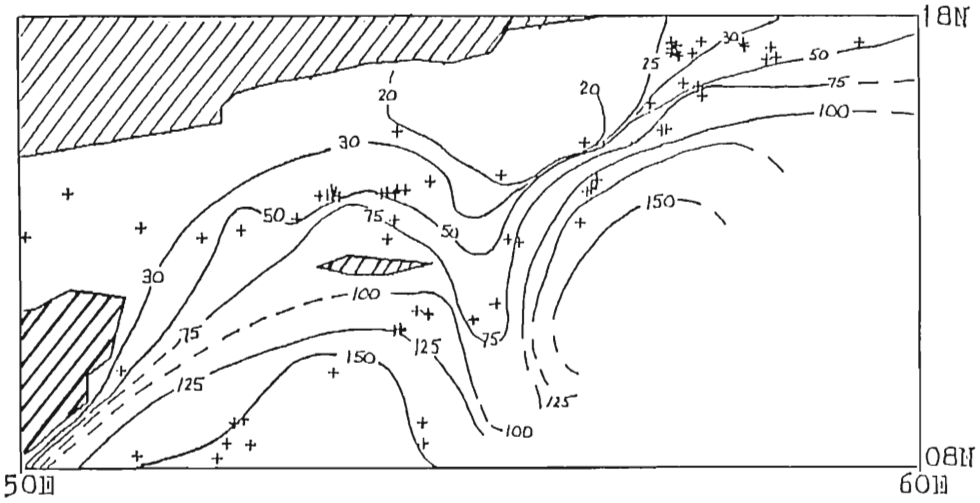

Fig. 25. The 18°C isotherm depth (meters) for 1 - 10 October 1985. Contours are generated from the BT data (solid contours) when sufficient readings are available, and are estimated (dashed contours) where BT data are deficient. Numerous dynamic features can be observed surrounding Socotra Island. The great whirl is seen penetrating from the south, while indications of the Socotra Eddy are observed by a deepening of the isotherm east of Socotra. The strong North Socotra Cyclonic Eddy is observed to the northeast of Socotra, with a relatively cool tongue extending to the south immediately east of the island, and separating the great whirl and Socotra Eddies. Weak deepening of the thermocline (warming) is observed to the north and west of Socotra, while intense fronts are observed off the coast of Somalia, northeast of Socotra, and between the Socotra Eddy and the intense North Socotra Cyclonic Eddy.

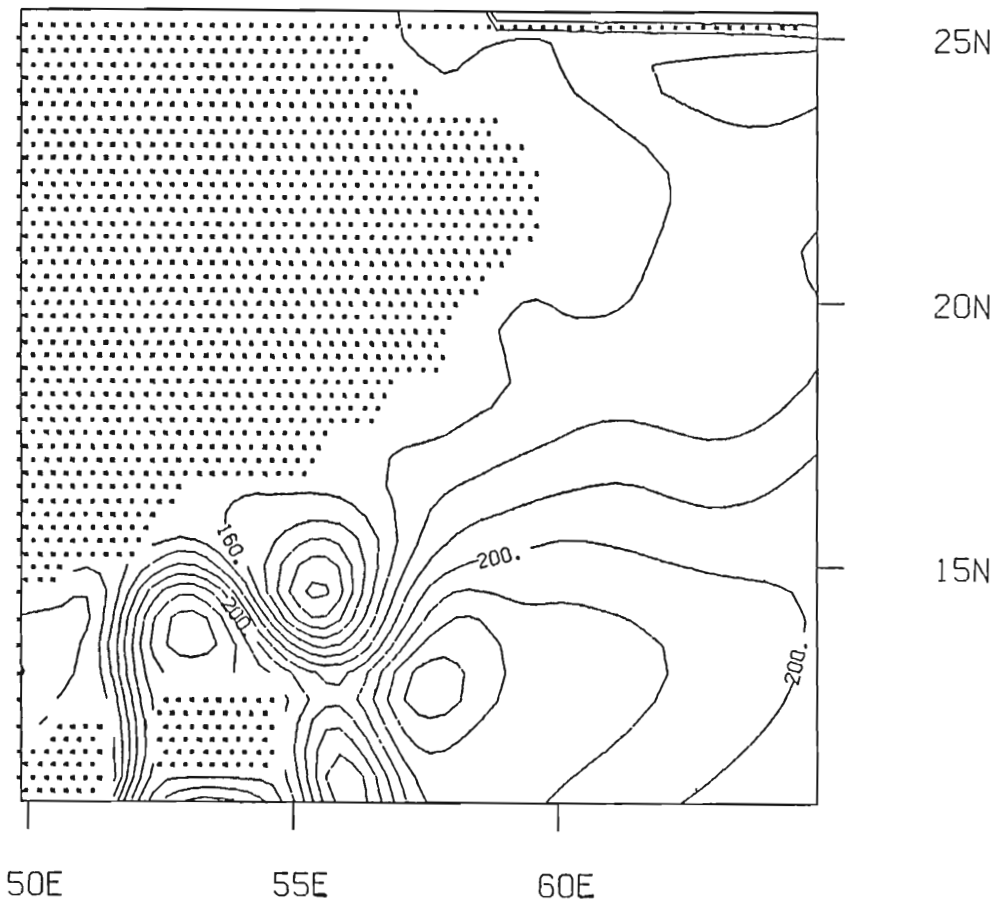

Fig. 26. Model response for 6 October 1985. The three major anticyclonic eddies - the great whirl, North Socotra Warm Eddy and Socotra Eddy - as well as the North Socotra Cyclonic Eddy are all well established around Socotra Island. A thin layer (cool) tongue extends south of the North Socotra Cyclonic Eddy east of Socotra, separating the three anticyclonic eddies from each other. Strong frontal boundaries are observed west of Socotra and the North Socotra Warm Eddy, and along the two boundaries separating the North Socotra Cyclonic Eddy from the Socotra and North Socotra Warm Eddies.

Eddy, and along the two boundaries separating the North Socotra Cyclonic Eddy from the Socotra and North Socotra Warm Eddies.

two figures along 14°N are shown in Fig. 27, confirming the model's accurate prediction and positioning of the North Socotra Warm Eddy, North Socotra Cyclonic Eddy, Socotra Eddy, and the intense frontal boundaries separating each. In fig. 28, profiles of the region further to the south display the remarkable accuracy of the model in predicting the great whirl's position and spacial dimension.

Towards the end of the month, there is an expansion to the northwest of the North Socotra Warm Eddy and slow westward drift, towards Socotra, of the Socotra Eddy. This latter effect is apparent in the 26 October model response, by the breakdown of the cool tongue east of Socotra into a strong frontal boundary to the north and a small cyclonic eddy to the south, Fig. 29. The contoured BT data for 20 - 30 October, Fig. 30, shows this effect, as the cool tongue contracts in the center, pinching off a small eddy to the south. Again, profiles of the model response and BT data along 14°N, Fig. 31, demonstrate a remarkable accuracy in the model.

For November, the model displays a slow weakening of the dynamic features developed during the fall (Fig. 32). The two cyclonic and three anticyclonic eddies established in the previous months maintain their respective positions throughout November, but all show signs of spacial spreading and weakening as the pycnocline flattens considerably. Strong fronts remain along the Gulf of Aden, and between the North Socotra Cyclonic Eddy and the Socotra and North Socotra Warm Eddies. but the great whirl and weak cyclonic eddy

between the North Socotra Cyclonic Eddy and the Socotra and North Socotra Warm Eddies, but the great whirl and weak cyclonic eddy

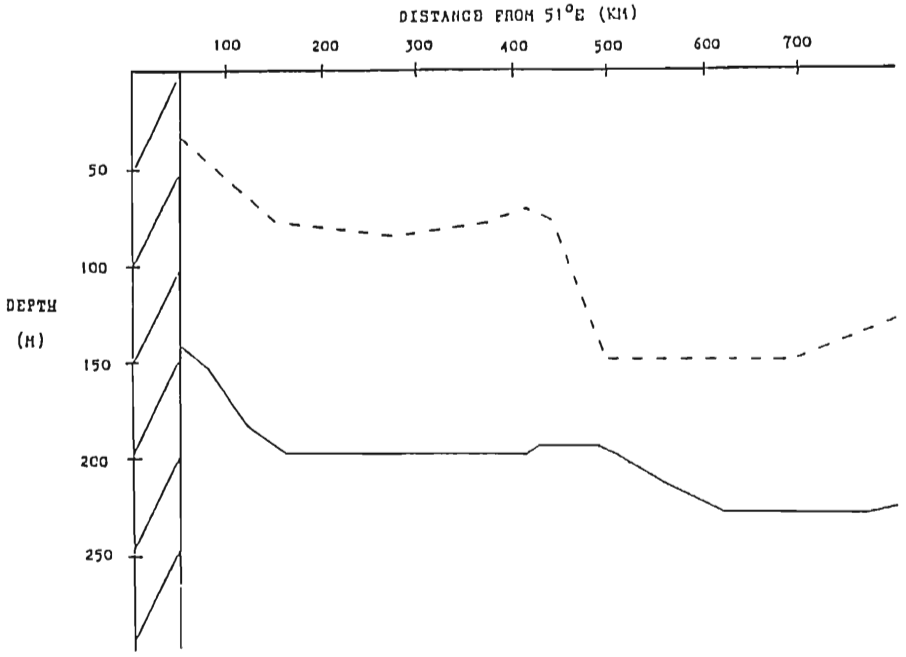

Fig. 27. Profiles of the BT 18°C isotherm for 1 - 10 October 1985 (dashed line) and the model ULT for 6 October 1985 (solid line), along 12°N. Distances are measured east from 51°E. Somalia extends over the first 50km. The strong front west of Socotra is observed at about 100km, followed by the cool tongue east of the island at about 400km, and the Socotra Eddy at about 500 - 600km. As seen here, the model reproduces these features quite well with respect to the actual data.

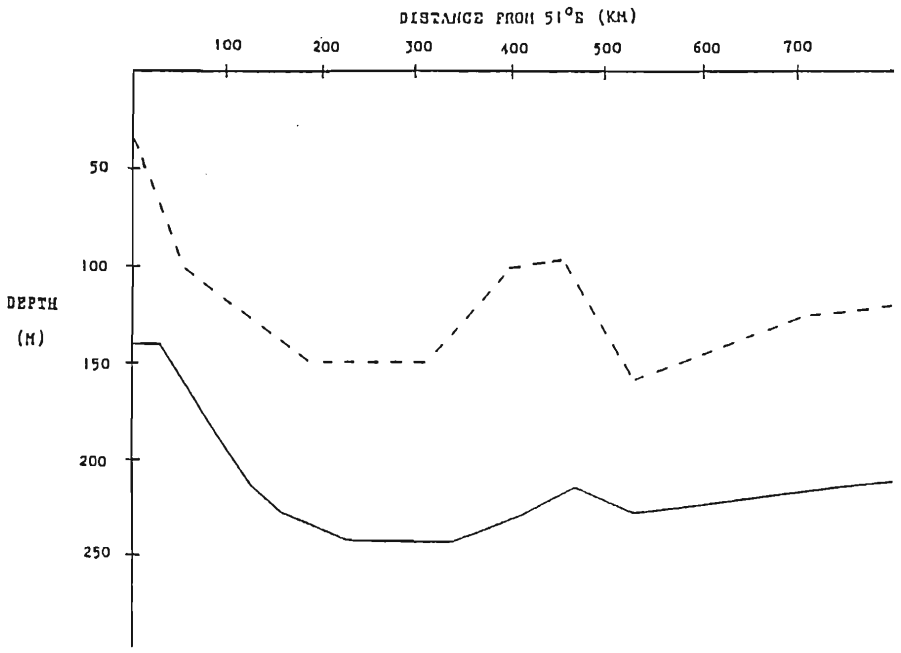

Fig. 28. Same as fig. 27, along 10°N. Again, the great whirl, cool tongue, and Socotra Eddy appear in each profile, with the model displaying remarkable accuracy.

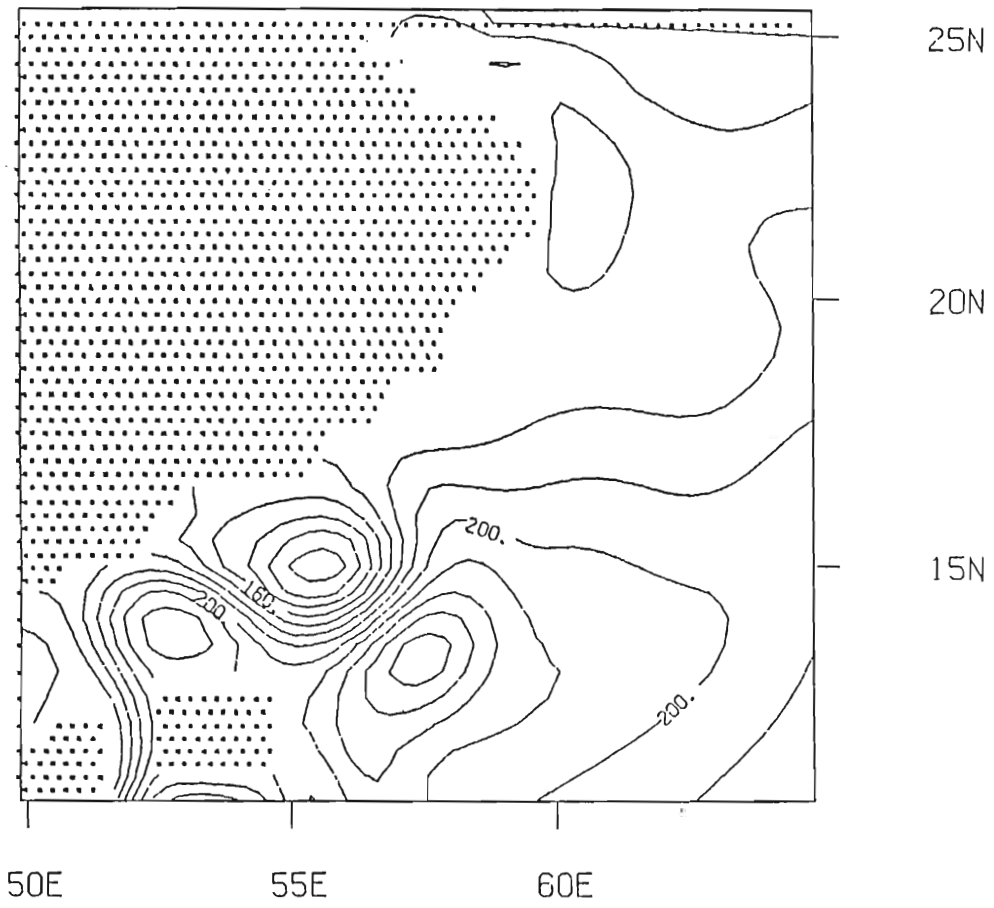

Fig. 29. Model response for 26 October 1985. The three anticyclonic eddies - great whirl, North Socotra Warm Eddy, and Socotra Eddy - are present around Socotra Island, separated by the well-developed North Socotra Cyclonic Eddy and the thin ULT (cool) tongue extending south from it along the eastern shore of Socotra. The Socotra Eddy has drifted westward and begun to squeeze out the cool tongue, as indicated by a thicker ULT filling east of Socotra, and a cyclonic eddy separating from the tongue southeast of the island. Strong fronts are again present west of Socotra and the North Socotra Warm Eddy and separating the North Socotra Cyclonic Eddy from the Socotra and North Socotra Warm Eddies.

eddy separating from the tongue southeast of the island. Strong fronts are again present west of Socotra and the North Socotra Warm Eddy and separating the North Socotra Cyclonic Eddy from the Socotra and North Socotra Warm Eddies.

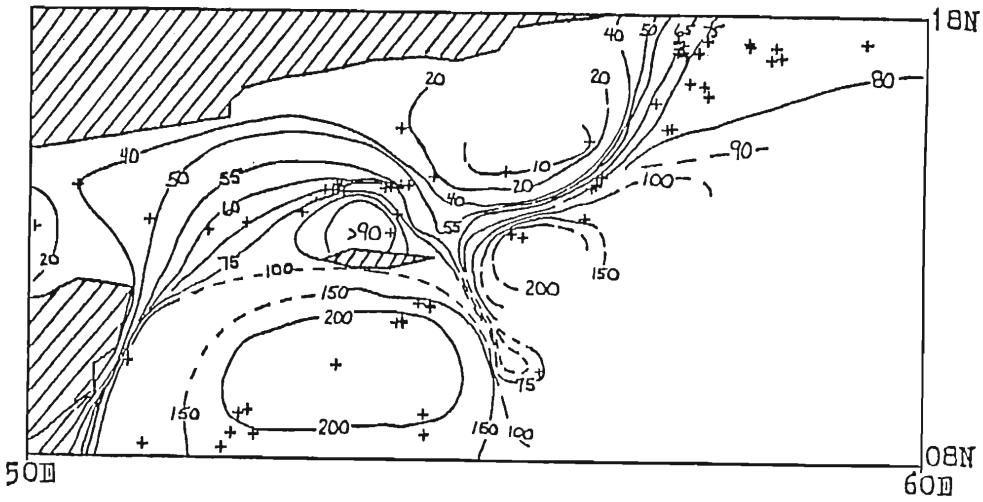

Fig. 30. The 18°C isotherm depth (meters) for 20 - 30 October 1985. Contours are generated from the BT data (solid contours) when sufficient readings are available, and are estimated (dashed contours) where BT data are deficient. The intense great whirl maintains itself to the south of Socotra while the Socotra Eddy continues to slowly migrate to the west. The North Socotra Warm Eddy has intensified and expanded to the northwest, almost touching the Arabian Peninsula. The North Socotra Cyclonic Eddy has also expanded and intensified, while the cool tongue to the east of Socotra is almost pinched off. Strong fronts occur off the coast of Somalia; between the North Socotra Warm Eddy, North Socotra Cyclonic Eddy, and Socotra Eddy; to the east of the North Socotra Cyclonic Eddy; and off the east coast of Socotra Island.

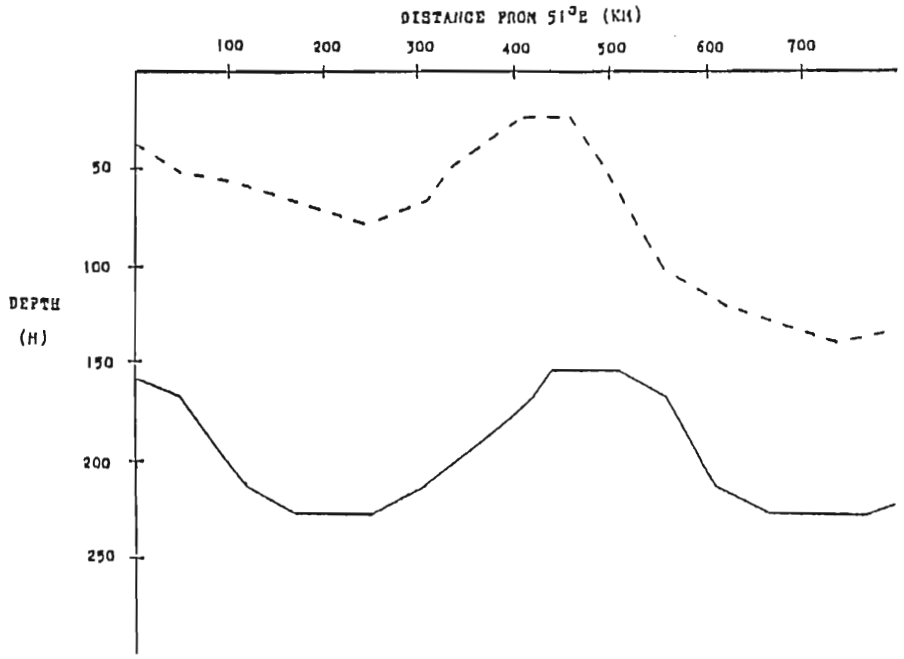

Fig. 31. Profiles of the BT 18°C isotherm for 20 - 30 October 1985 (dashed line) and model ULT for 26 October 1985 (solid line), along 14°N. Distances are measured east from 51°E. The cool water of the Gulf of Aden, the North Socotra Warm Eddy (250km), North Socotra Cyclonic Eddy (450km), and Socotra Eddy (700km) are clearly evident in their respective positions in each profile. The three strong frontal boundaries separating these four major features also appear in both profiles.

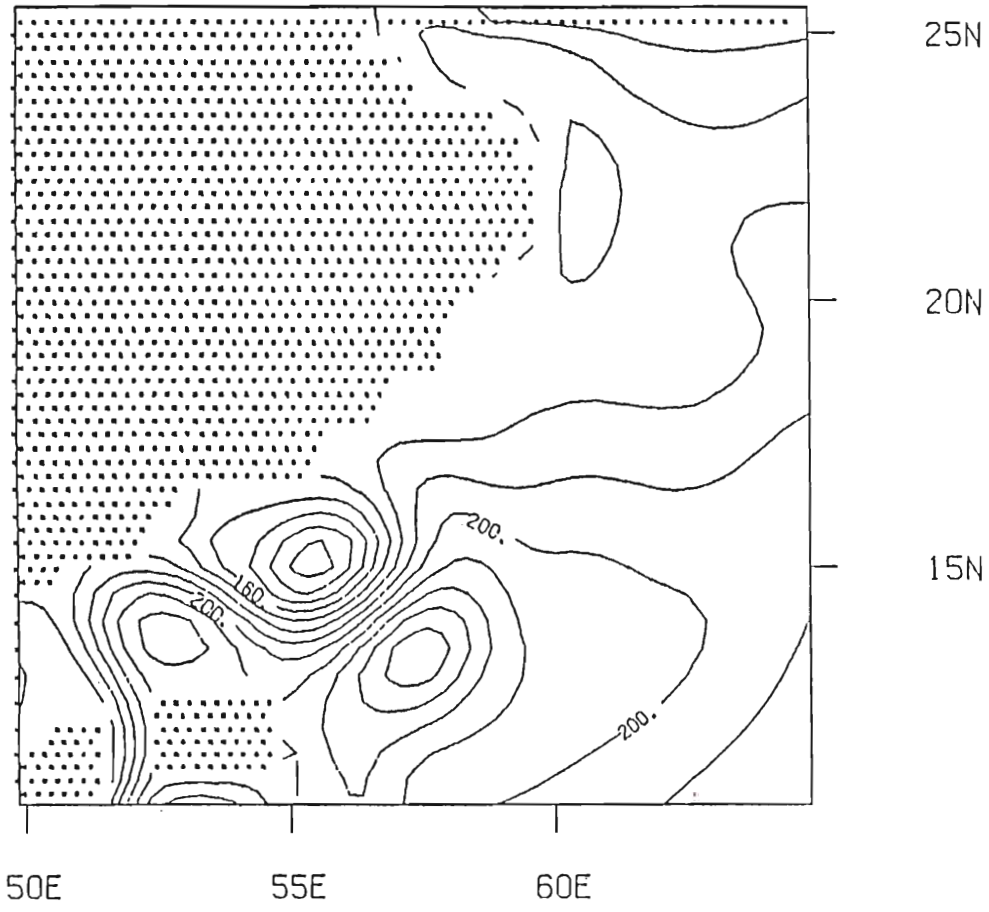

Fig. 32. Model response for 1 November 1985. Similar to fig. 28, except that the Socotra Eddy has drifted slightly closer to Socotra Island, while the thin ULT pocket off the Omani coast has contracted further to the north. Warmer water from the Gulf of Oman penetrates along the coast of the Arabian Peninsula from the north, and merges with warm water pumped in by the Socotra Eddy from the south.

southeast of Socotra deteriorate significantly, and are almost indistinguishable by the end of the month.

In Fig. 33, the NOAA-9 sea surface temperature satellite image of 2 November is compared with the 1 November model response along 14.5°N. The resultant profiles again show the accurate placement of the North Socotra Warm Eddy, North Socotra Cyclonic Eddy, Socotra Eddy, and associated frontal boundaries separating these features.

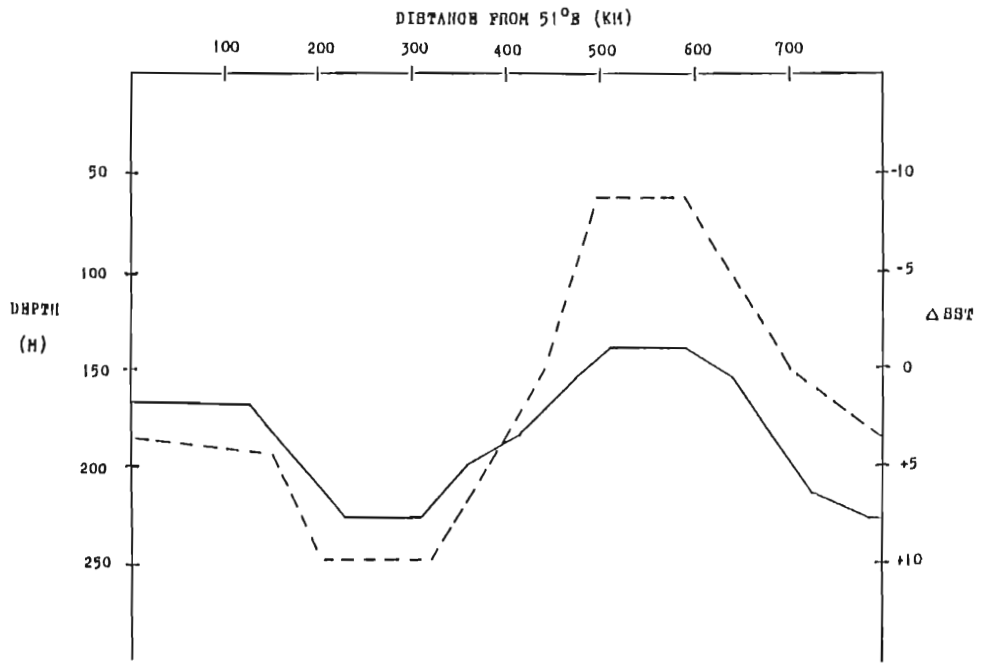

Fig. 33. Profiles depicting sea surface temperature anomalies from the NOAA-9 AVHRR image of 2 November 1985 (dashed line) and the model upper layer depth for 1 November 1985 (solid line). Distances are measured east from 51°E along 14.5°N. Again the curves display remarkable consistancy, showing the North Socotra Warm Eddy at about 250km, the North Socotra Cyclonic Eddy at about 550km, the Socotra Eddy at about 800km, and strong frontal boundaries separating these major features at 200km, 400km, and 700km respectively.

CONCLUSIONS AND DISCUSSION

This study has confirmed that the fall circulation pattern of the northwest Arabian Sea is strongly influenced by the transition of the region from the regime of the summer southwest monsoon to that of the winter northeast monsoon. The strong eddies and fronts generated during July and August, at the height of the southwest monsoon, persist throughout the period and respond to the influence of the rapidly reversing winds and surface current.

Throughout the study, in which forcing was provided by 1985 observed winds, the model has proven quite effective in its ability to reproduce the upper layer ocean structure observed in 1985. In particular, around Socotra Island, a region dominated by robust features - the great whirl to the south, Socotra Eddy to the east, North Socotra Cyclonic Eddy to the northeast, and North Socotra Warm Eddy to the northwest - the model is extremely comparable to the observational data, with each of the four principle eddies well represented, both spacially and temporally. Off the coast of Oman, however, where the dynamic structure is characterized by relatively weak flows and a large region of relatively homogeneous ULT, the model is less effective. Small-scale structures overlaying the dominant gradual thickening of ULT offshore, while clearly evident in the observational data, are absent from the model. Instead, the model gradual thickening of ULT offshore, while clearly evident in the observational data, are absent from the model. Instead, the model represents the area as a large region of relatively constant ULT.

Model resolution, which is approximately 30km at this latitude, in conjuction with the weak nature of the flow, probably is responsible for much of the model's difficulty here.

Also absent from the model is the thin region of upwelling clearly present in the data. Again, model resolution likely is a factor, however coastal topography, which in reality fluctuates dramatically from a wide shelf along Ras ash Sharbát and around Masiráh Island to a very narrow shelf along Ras Marbat, probably plays a significant role in the presence and structure of this upwelling. Again, this effect is not represented in the model. Similarly, the effects of thermodynamics may also serve as a potential source of error, as the summer-heated waters of the Persian Gulf and Gulf of Oman, (where September SST frequently exceeds 30°C) likely impart an influence on the continuity of the upper layer structure off the Omani coast. This is also not accounted for in the model, though it probably is less important than the resolution and topography effects.

Regardless, the fluctuations observed in the data off the Omani coast are quite small, on the order of tens of meters over the entire 750,000 km^2 region, and when compared to the robust features found around Socotra, appear to be of only minor significance. Hence, the model does provide a very reasonable hindcast of the dynamic structure observed in the fall of 1985.

Further model improvement is both possible and desirable. As observed in the fall of 1985.

Further model improvement is both possible and desirable. As discussed above, inclusion of coastal topography and thermodynamic

effects may vastly improve the model's accuracy in regions of weak flow and relatively constant horizontal structure. Additionally, the expansion of the model geometry to include the entire Indian Ocean basin, presently underway, should improve the model's results, as remote forcing, particularly from the Southern Hemisphere trade winds will exert a greater influence on the model response. Multi-level vertical structure would also be useful in determining vertical shearing and entrainment effects on the upper layer circulation.

A number of recommendations can be made to enhance further verification studies. Of foremost concern in any assessement must be the availability of corroborating data. While the limited data available for this study was sufficient, coverage of specific areas of interest would have both simplified and improved the analysis; for example, better BT coverage east of Socotra could have improved the analysis of the cool tongue present east of Socotra in the model in October. Nighttime channel 3 AVHRR imagery, much less susceptible to moisture contamination than the channel 4 imagery used in this study, would also certainly improve the availability and quality of the data and would greatly assist in determining surface circulation structure. Finally, verification studies should be attempted when drifters, buoys, phytoplankton, and other observational data are all available concurrently. This requires close interaction between modelers and observationalists to ensure a unified and successful effort.

modelers and observationalists to ensure a unified and successful effort.

Despite the limited resources available for this study, it has provided a useful insight into the model's effectiveness, and is an important evolutionary step in the model's development. It has shown the ability of this simple 1½ layer model to reproduce accurately the robust features of the Arabian Sea when provided accurate observed wind data, and justifies further model improvement and sophistication. More importantly, it has demonstrated the ability of the model to use near real-time winds to reproduce accurately Arabian Sea dynamics, and sets the stage for the possible forecasting in near real-time of the region's ocean dynamics when scatterometer winds become available early in the next decade.

REFERENCES

Anderson, D. L. T., The Somali Current, Ocean Modelling, 34, 6-9, 1981 (unpublished manuscript).

Anderson, D. L. T. and D. W. Moore, Cross-equatorial jets with special relevance to very remote forcing of the Somali Current, Deep Sea Res., 26, 1-22, 1979.

Anderson, D. L. T. and P. B. Rowlands, The Somali Current response to the monsoon: the relative importance of local and remote forcing, J. Marine Res., 34, 395-417, 1976.

Brown, O. B., J. G. Bruce, and R. H. Evans, Evolution of sea surface temperature in the Somali Basin during the southwest monsoon of 1979, Science, 209, 595-597, 1980.

Bruce, J. G., Large scale variations of the Somali Current during the southwest monsoon, Deep Sea Res., 20, 837-846, 1973.

Bruce, J. G., Eddies off the Somali coast during the southwest monsoon, J. Geophys. Res., 84 (C12), 7742-7748, 1979.

Bruce, J. G., The wind field in the western Indian Ocean and the related ocean circulation, Mon. Weather Rev., 111, 1442-1452, 1983.

Cadet, D. L. and B. C. Diehl, Inter-annual variability of surface fields over the Indian Ocean during recent decades, Mon. Wea. Rev., 112, 1921-1935, 1984.
fields over the Indian Ocean during recent decades, Mon. Wea. Rev., 112, 1921-1935, 1984.

Cagle, B. J. and R. Whritner, Arabian Sea project of 1980 - Composites

of infrared images, Technical report, Office of Naval Research, Western Regional Office, Pasadena, Ca., 1-61, 1981.

Camerlengo, A. L. and J. J. O'Brien, Open boundary conditions in rotating fluids, J. Comput. Phys., 35, 12-35, 1980.

Charney, J. G., The generation of ocean currents by the wind, J. Mar. Res., 14, 477-498, 1955.

Cox, M. D., A mathematical model of the Indian Ocean, Deep Sea Res., 17, 47-75, 1970.

Cox, M. D., Equatorially trapped waves and the generation of the Somali Current, Deep Sea Res., 23, 1139-1152, 1976.

Cox, M. D., A numerical study of Somali Current eddies, J. Phys. Oceanogr., 9, 311-326, 1979.

Cox, M. D., A numerical study of surface cooling processes during summer in the Arabian Sea, Monsoon Dynamics, Ch. 36, edited by M. J. Lighthill and R. P. Pearce, Cambridge Univ. Press, 735 pp., 1981.

Findlater, J., Mean monthly airflow at low levels over the western Indian Ocean, Geophys. Mem., No. 115, 53 pp., 1971.

Findlay, A. G., A Directory for the Navigation of the Indian Ocean, Richard Holmes Laurie, London, 1062 pp., 1866.

Hellerman, S. and M. Rosenstein, Normal monthly wind stress over the world ocean with error estimates, J. Phys. Oceanogr., 13, 1093-1104, 1983.

Hurlburt, H. E., and J. D. Thompson, A numerical model of the Somali

1104, 1983.

Hurlburt, H. E., and J. D. Thompson, A numerical model of the Somali

Current, J. Phys. Oceanogr., 6, 646-664, 1976.

Knox, R. A., and D. L. T. Anderson, Recent advances in the study of low-latitude ocean circulation, Prog. Oceanogr., 14, 259-318, 1985.

Leetmaa, A., D. R. Quadfasel and D. Wilson, Development of the flow field during the onset of the Somali Current, J. Phys. Oceanogr., 12, 1325-1342, 1982.

Legler, D. M., I. M. Navon, and J. J. O'Brien, A direct minimization approach to objective analysis of pseudo-stress over the Indian Ocean, (in preparation).

Lighthill, M. J., Dynamic response of the Indian Ocean to onset of the southwest monsoon, Phil. Trans. Roy. Soc. London, Series A, 265, 45-92, 1969.

Lin, L. B., and H. E. Hurlburt, Maximum simplification of nonlinear Somali Current dynamics, Monsoon Dynamics, Ch. 37, edited by M. J. Lighthill and R. P. Pearce, Cambirdge Univ. Press, 735 pp., 1981.

Luther, M. E., and J. J. O'Brien, A model of the seasonal circulation in the Arabian Sea forced by observed winds, Prog. Oceanogr., 14, 353-385, 1985.

Luther, M. E., J. J. O'Brien, and A. H. Meng, Morphology of the Somali Current system during the southwest monsoon, Coupled Ocean-Atmosphere Models, Ch. 27, edited by J. C. J. Nihoul, Elsevier Science Publishers B. V., Amsterdam, 405-437, 1985.
Atmosphere Models, Ch. 27, edited by J. C. J. Nihoul, Elsevier Science Publishers B. V., Amsterdam, 405-437, 1985.

Schott, F., Monsoon response of the Somali Current and associated upwelling, Prog. Oceanogr., 12, 357-382, 1983.

Schott, F., and D. R. Quadfasel, Variability of the Somali Current system during the onset of the southwest monsoon, J. Phys. Oceanogr., 12, 1343-1357, 1982.

Swallow, J. C. and M. Fieux, Historical evidence for two gyres in the Somali Current, J. Mar. Res., 40 (suppl.), 747-755, 1982.

Swallow, J. C., R. L. Molinari, J. G. Bruce, O. B. Brown and R. H. Evans, Development of near-surface flow pattern and water mass distribution in the Somali Basin, in response to the southwest monsoon in 1979, J. Phys. Oceanogr., 13, 1398-1415, 1983.